Received: 17 October 2021 | Revised: 11 July 2022 | Accepted: 15 July 2022

DOI: 10.1002/eqe.3717

RESEARCH ARTICLE

WILEY

Influence of the design objectives on the seismic performance of steel moment resisting frames retrofitted with buckling restrained braces

Fernando Gutiérrez-Urzúa | **Fabio Freddi**

Department of Civil, Environmental & Geomatic Engineering, University College of London, London, UK

Correspondence
Fernando Gutiérrez-Urzúa, Department of Civil, Environmental & Geomatic Engineering, University College of London, London WC1E 6BT, UK.
Email: f.urzua@ucl.ac.uk

Funding information
Consejo Nacional de Ciencia y Tecnología, Grant/Award Number: CONACYT-FiiDEM2018-000013-01EXTF-00148

Abstract

Buckling restrained braces (BRBs) represent an effective strategy for the seismic retrofit of existing steel moment resisting frames (MRFs), as they contribute to increasing the strength and ductility capacity of the structure. However, current design strategies do not provide recommendations on how the performance increase is achieved. Prioritising either the increase of strength or ductility capacity has an impact on the damage evolution and affects the overall performance of the structure. A low increase of strength typically requires larger exploitation of the ductility capacity (i.e., damage) of the existing structure, while a high increase of strength produces a significant increase of stiffness, which is often accompanied by an increase of the seismic demands that may limit the effectiveness of the retrofitting solution. The present study assesses the impact of these decisions on the overall performance of steel MRFs retrofitted with BRBs. For this purpose, two MRFs with several BRB retrofitting configurations are used as case study structures. Finite Element Models are built in OpenSees and assessed through Incremental Dynamic Analyses to account for the record-to-record variability. Fragility relationships are derived based on local Engineering Demand Parameters (EDPs) to describe structural and non-structural damage, as well as path-dependent damage indicators (i.e., residual drifts and cumulative ductility in BRBs). A comparison of the overall performance of the structures is carried out in terms of risk estimates for a high seismicity location.

KEYWORDS
buckling restrained braces, design objectives, local engineering demand parameters, moment resisting frames, risk assessment, seismic retrofit

1 | INTRODUCTION

Steel moment resisting frames (MRFs) represent a popular structural typology for seismic-resistant buildings due to their architectural and constructional advantages (e.g., open facades, fast construction); nonetheless, several performance

limitations have been identified in these structures after strong ground motions.[1–3] Although these deficiencies have been addressed in modern design codes (e.g., AISC 341-16[4]), a significant number of existing steel MRFs were designed according to older regulations and are often found in need of performance upgrades.[5] Among the retrofitting options, an increasingly popular approach consists in the inclusion of Buckling Restrained Braces (BRBs) within the frames of the existing structure (e.g., 6–10) as these devices can provide additional strength, stiffness, and energy dissipation capacity.[11,12] Unlike regular braces, BRBs can develop significant compression capacity thanks to an unbonded restraining sleeve that limits the steel core from buckling, thus dissipating the seismic energy with nearly symmetrical hysteretic loops.[13,14]

Modern seismic retrofitting codes (e.g., ASCE 41-17[15]) and seismic design codes (e.g., AISC 341-16, ASCE 7–16[16]) have incorporated general guidelines for the design of Buckling Restrained Braced Frames (BRBFs). These include requirements related to capacity design (e.g., the capacity of connections and adjacent elements larger than BRB's capacity), BRB device characteristics, deformation limits (e.g., strain limits, plastic deformation limits, storey drift limits), testing protocols, frame configurations and other general design considerations (e.g., R-factors and m-values for linear approaches). Nonetheless, they offer design freedom in deciding how the structure meets the seismic demand through retrofitting; hence, the design can be aimed at increasing the strength or deformation capacity of the structure. The retrofitting of MRF with BRBs results in a dual system with increased strength and plastic deformation capacity (and, consequently, ductility and stiffness) with respect to the existing structures through the addition of BRBs. To simultaneously consider both characteristics in the design process, the capacity curve of the structure can be compared to the ductility-reduced (e.g., inelastic) demand spectrum in the Acceleration-Displacement Response Spectrum (ADRS) plane, as previously done by several other authors (e.g., 17, 18). Several design methods have been developed for newly designed BRBFs and for the retrofitting of existing structures with BRBs (e.g., 19–22). The present study uses a design procedure aligned with the one developed by Ragni et al.,[20] as it allows to directly calibrate strength, stiffness and ductility of the BRBs in order to meet specific design objectives. Nonetheless, prioritising either strength or deformation capacity may allow simultaneously reaching other performance objectives. For example, the inclusion of "large" BRBs (i.e., large yielding strength and stiffness) can limit the deformations, thus protecting the structural members in the MRF[6,7,23] and the non-structural components of the existing structure[9]; however, it also affects the dynamic response of the structure, which could be accompanied by an increase in the seismic demands,[7,9] and a redistribution of forces that would require local retrofitting interventions. On the other hand, the inclusion of "small" BRBs (i.e., low yielding strength and stiffness) allows the engagement of the existing MRF in the dissipation of the seismic energy, attenuates the increase of the seismic demands and represents a lower investment due to smaller bracing systems and minor local retrofitting requirements. Nonetheless, this second option may result in difficult repairability of the structure after a strong earthquake due to large permanent drifts[23,24] and damage to the existing structural and non-structural elements.

The complexity of designing BRBFs is further highlighted when considering the proclivity of BRB devices to fail due to low-cycle fatigue,[23,25–27] their ability to develop isotropic hardening,[14] and the possibility of inducing large residual drifts in the structure[24] as all of these effects are path-dependent. In the present work, these aspects are considered through a probabilistic-based assessment procedure accounting for the uncertainty related to the record-to-record variability. Several studies have made use of fragility curves to relate the probability of exceeding a predefined damage state or failure condition to a strong-motion shaking severity, quantified by means of an appropriately selected Intensity Measure (IM). For instance, Castaldo et al.[9] and Güneyisi[6] investigated the seismic performance of low-rise structures retrofitted with BRBs. For this purpose, fragility curves were used, and comparisons were drawn in terms of risk estimates to consider the shift in demands due to the change in modal properties of the structure. Despite the influence that the design choices may have on the performance of a (demand-compliant) retrofitted structure, the aforementioned works have focused on increasing the seismic performance of a structure to meet its demands and to compare it to the un-retrofitted case, thus overlooking the effects that the design decisions have on the performance of the retrofitted building itself. Only a few authors have performed parametric analyses to understand the effect of the design decisions (e.g., 23); nonetheless, they have been mostly focused on Single Degree of Freedom (SDoF) systems, which overlooked local performance aspects.

The performance of the structure is conventionally evaluated based on Engineering Demand Parameters (EDPs)[28] and the comparison between their demand values and acceptance criteria (also referred to as capacity limits). Most research studies focusing on fragility assessment (e.g., 6, 7, 9, 29) consider global EDPs, as they allow estimating structural and non-structural damage states with relatively low computational efforts. Among others, the inter-storey drift ratio (IDR) is a widely adopted global EDP, as it is used as a proxy to synthetically describe the local damage in the structure. However, as highlighted in previous studies (e.g., 5, 7), the proportionality between local and global EDPs is not necessarily held in all cases. In addition, the definition of acceptance criteria for IDR at each performance level adds epistemic uncertainty to the fragility relationships, as they are either established based on code- or literature-based generic structural limits (e.g., 6) or through mapping processes that rely on simplified correlations (e.g., 30). Thus, the present study makes use of local

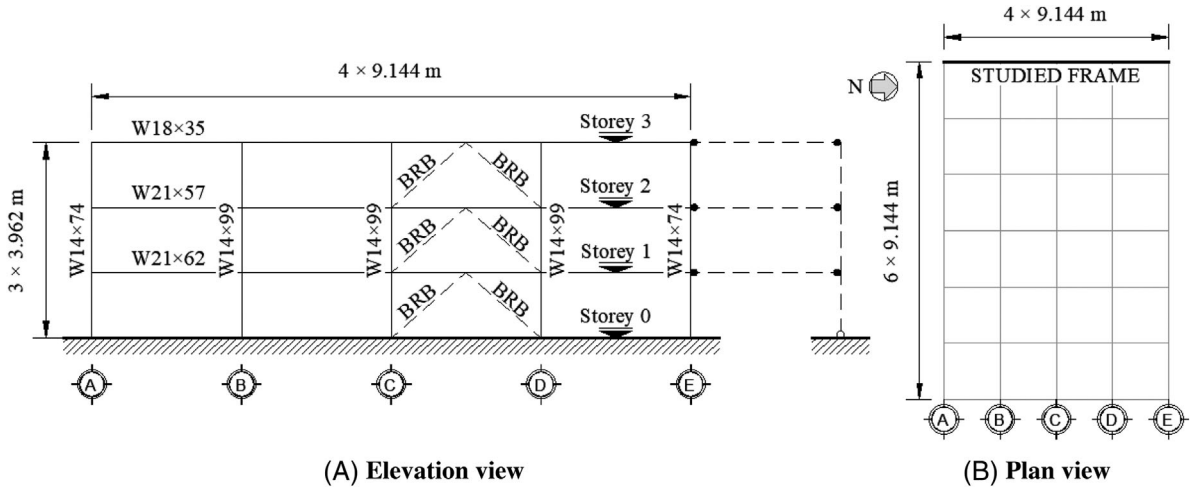

FIGURE 1 Case study structure A (representative of an existing low-rise steel MRF): (A) elevation view, (B) plan view

EDPs, which allow capturing the structural damage on each element individually, including interaction effects (e.g., axial loads reducing rotation capacity of columns), to correctly attribute the deformation contribution of elements working in series (e.g., beams and panel zones), to detect undesired mechanisms (e.g., soft-storey mechanism) and to quantify the energy dissipation and Cumulative Ductility Demand (CDD) on each BRB.

The present study investigates the effect of the design objectives (e.g., design target drift, hence, BRBs sizing) on the performance of steel MRFs retrofitted with BRBs by comparing several retrofit configurations. These design objectives are established in terms of target top storey drift (d_u) values. Two steel MRFs are selected as case study structures to represent two building categories: a low-rise (3 storeys) and a mid-rise building (6 storeys). Fragility relationships are derived considering local (i.e., component-level) EDPs, to measure the structural damage, global EDPs, to characterise the non-structural damage, and path-dependent quantities (i.e., residual drifts and cumulative ductility in BRB devices) to assess the repairability of the case study structures. Finally, risk estimates are derived for each EDP and performance level by accounting for the seismic hazard related to a high-seismicity region to draw comparisons on the performance of different retrofitting schemes.

2 | ASSESSMENT AND RETROFITTING METHODOLOGY

The present section presents the methodology followed for the assessment and retrofitting design of each case study structure. However, to avoid unnecessary repetition, some details are only presented for the low-rise building, referred to as case study structure A, while later sections present the results for both case study structures.

Case study structure A is based on the pre-Northridge Boston 3-storey structure designed within the SAC Steel Project.[31] This structure is considered to be representative of low-code steel MRFs, as it was designed following the provisions of the 12th edition of the National Building Code[32] by considering gravity, wind and low seismic demands. This case study structure was designed assuming stiff soil (site Class D in modern standards, e.g., 15, 16), office occupancy, regular plan distribution and no considerable irregularities along with the height. In addition, only the perimeter frames are considered to withstand lateral loads (i.e., internal frames are connected as gravity frames only), as it was common practice in the early 1990 s in the US. In this study, only one of the North-South external MRFs is considered, as the building is fully symmetric. The material properties for beams and columns are based on the ASTM A572standard, specifically steel Grade 50 (Group 1 f_y = 344.74 MPa; E = 199.95 GPa). The nominal value of f_y is further increased by 10% to account for the material overstrength (i.e., to consider the expected yielding strength, f_{ye}), based on the recommendations of ASCE 41-17. Details of this frame are shown in Figure 1.

The retrofitting aims at improving the seismic performance of the structure to comply with larger seismic demands, as is the case when there is a change in the occupancy of the building (e.g., housing occupancy to school occupancy) or there is an update to the hazard maps and/or code regulations. For this purpose, the seismic hazard characteristics associated with Los Angeles (site Class D) are considered, as they are representative of a site with high seismicity. The retrofitting is carried out by including two BRBs per storey in a chevron (i.e., inverted "V") configuration, as shown in Figure 1(A).

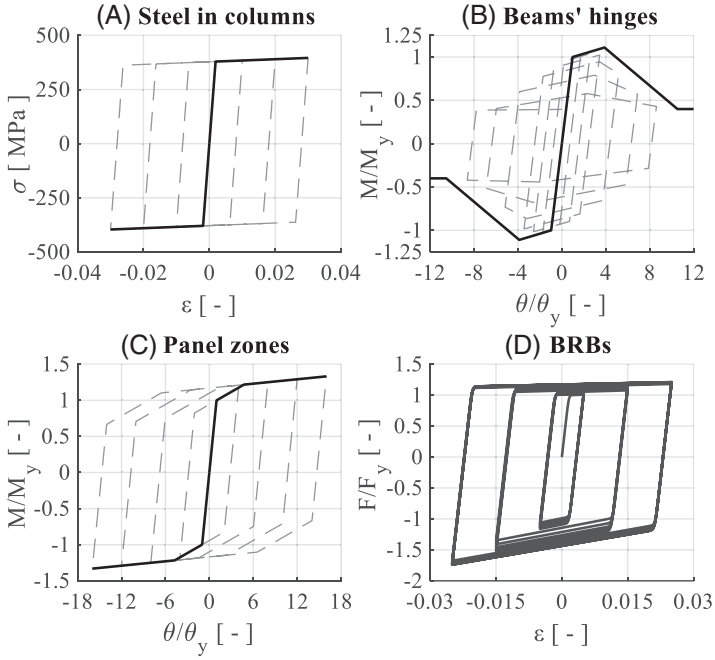

FIGURE 2 Monotonic and cyclic behaviour in the OpenSees model for (A) steel in columns (i.e., fibres) with $\beta = 0.003$; (B) beams' hinges; (C) panel zones with $\beta = 0.01$; and (D) BRB devices with $\alpha = 10$, $\delta = 0.2$, $\beta_T = 0.0025$ and $\beta_C = 0.02$

Each BRB is composed of a pinned in-series arrangement of a BRB device and an Elastic Brace (EB). The nominal yield strength of the material used for the BRB device core is considered as $f_y = 322$ MPa. The Young's modulus of the BRB device and EB is considered as E = 199.95 GPa.

2.1 | Finite element modelling

A 2-D nonlinear finite element model of the perimeter MRF is developed in OpenSees.[33] As only one of the external frames is considered, only half of the storey masses are assigned to the studied frame (i.e., 957/2t for the 1st and 2nd storeys, 1035/2t for the 3rd storey). Gravity loads applied on the case study structure correspond only to the tributary area of the considered external frame. Columns are modelled based on the distributed plasticity approach to account for the interaction of axial and bending stresses. Beams are modelled based on the lumped plasticity approach (i.e., nonlinear rotational springs plus an elastic beam element). The plastic hinges on the beams are calibrated based on the model proposed by Lignos and Krawinkler,[34] modified as suggested by Zareian and Medina[35] to compensate for the flexibility and damping properties of the beams. Panel zones are modelled according to the 'Scissors model'[36] using two parallel rotational springs. Column bases are modelled as fixed, as previous studies[37] have suggested that MRFs modelled with a fixed base assumption do not exhibit significantly different behaviour when compared to frames modelled with detailed base plate springs. Damping is considered by using mass- and stiffness-proportional (i.e., Rayleigh) damping, with a damping ratio $\zeta = 3\%$ for the first and second modes.

Figure 2 shows the hysteretic behaviour of the aforementioned materials and components. Figure 2(A) shows the hysteretic behaviour of the steel material used in the columns' fibres modelled by using the *Steel01* Opensees material, with a post-yielding hardening (β), equivalent to 0.3% of the Young's modulus (E) and no cyclic degradation. Figure 2(B) shows the hysteretic behaviour of the beam system (i.e., the nonlinear plastic hinge spring and the elastic beam element), connected in series. The nonlinear spring's behaviour is modelled using the *Bilin* material (Modified IMK deterioration model).[38] Panel zones are modelled with *Steel01* and $\beta = 1\%$ hardening. As a result of the spring configuration, the trilinear curve shown in Figure 2(C) is a result of both springs working in parallel. Similarly to the columns, this component does not consider cyclic degradation.

The modelling approach of the BRBs (including BRB device and EB) is detailed in Figure 3. The BRB devices are modelled using axial-only *corotTrussSection* elements, characterised by the *SteelBRB* material,[14] while the EBs are modelled using *elasticBeamColumn* elements, as they are calibrated based on stiffness demands and checked to avoid yielding. An additional *elasticBeamColumn* support element is placed in parallel to each BRB device element in order to provide stability in other degrees of freedom. This element is characterised by high flexural stiffness and no axial capacity. Figure 2(D)

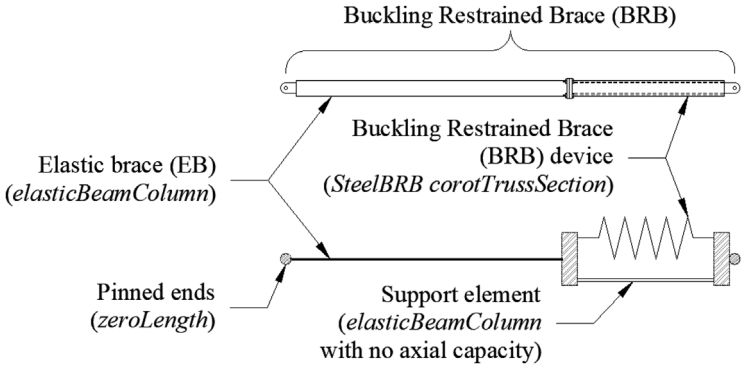

FIGURE 3 Modelling approach for the braces, including the BRB device, the EB and the support element

details the generic hysteretic behaviour of the BRB device element, with hardening parameters calibrated on previous experimental tests.[30]

The addition of the bracing system creates a truss-like cantilever mechanism composed of the added braces and the existing columns and beams (i.e., a BRBF). As the beam-to-column connections continue to provide a parallel load-transfer path for the structure, the lateral load-resisting mechanism is formed by a dual system.[23] Although some codes require the MRF to provide a non-negligible lateral capacity to the system (e.g., 25% in the ASCE 7–16), the present paper refers to the retrofitted structures as dual systems, regardless of the relative contribution of the MRF.

The gravity loads tributary to the non-modelled frames are lumped into a parallel continuous leaning column, similar to the approach followed by MacRae et al.,[39] as represented in Figure 1(A). The leaning column is linked to the structure by rigid truss elements. The objectives of the leaning column are (1) to account for the second-order geometric effects due to gravity loads (P-Δ), and (2) to provide continuous lateral stiffness (i.e., spine effects) along with the height of the structure. The latter issue is especially significant for low-code designed structures, as the stiffness of the gravity frame could represent a large portion of the overall lateral stiffness.[5] Each gravity column from the mass tributary area in the frame (i.e., half of the gravity columns in the building) is modelled as an individual nonlinear fibre-based element and connected within the same vertical axis. Despite modelling the columns individually, all the elements are connected to the same nodes acting as a spine element for the structure. This approach effectively functions as a single leaning column in which their geometric properties are added together; simultaneously, they can be monitored individually. The effects of the beam-to-column shear connections in the gravity frames can be significant in certain buildings, particularly when the contribution of the uncracked floor slab is considered in the low performance levels.[40] Nonetheless, the stiffness provided by these shear connections in the case study structures is negligible when compared to the contribution provided by the continuity of the gravity columns.[41] For this reason, the beam-to-column connections of the gravity frame are assumed as pinned in the present study.

As the base plates for gravity frames tend to be more flexible than those in the main frame, the modelling of the column bases for the leaning columns is often assumed as pinned. However, this assumption reduces the lateral stiffness of the gravity columns at the bottom storey, which leads to a large concentration of demands in the columns of the seismic-resistant perimeter MRF where the columns are fixed. To reduce this effect, the strength and stiffness of the base plates in the gravity columns are considered in the numerical model by adding *zeroLength* rotational springs, which properties are calibrated based on the approach proposed by Kanvinde et al.[42] As the literature describing the design of the considered case study structures does not include detailing on the base connections of the gravity frame, these elements are designed by following the approach suggested by the AISC Steel Design Guide.[43]

2.2 | Assessment of the existing structure

The retrofit design objectives are established by assessing the seismic performance of the bare frame through a first-mode proportional pushover analysis. The deformation demands imposed on local elements within the MRF (i.e., chord rotation in beams, chord rotation in columns, and distortion in panel zones) are recorded during the pushover analysis and compared to the deformation-based acceptance criteria established in the ASCE 41-17 and summarised in Table 1. For each element type, the ASCE 41-17 defines acceptance criteria at three structural performance levels: (1) the Immediate Occupancy (IO) structural performance level, where the structure is safe to occupy and retains its original strength and

TABLE 1 Plastic deformation acceptance criteria according to ASCE 41-17

Element type	Immediate Occupancy (IO)	Life Safety (LS)	Collapse Prevention (CP)
Beams	1 to 2.25 θ_y	3 to 9 θ_y	4 to 11 θ_y
Panel zones[1]	1 θ_y	12 θ_y	12 θ_y
Columns[2]	0.5 a	0.75 b	b

[1]For panel zones with $|\nu_G| < 0.4$.
[2]For definition of 'a' and 'b' refer to ASCE 41-17.[15].

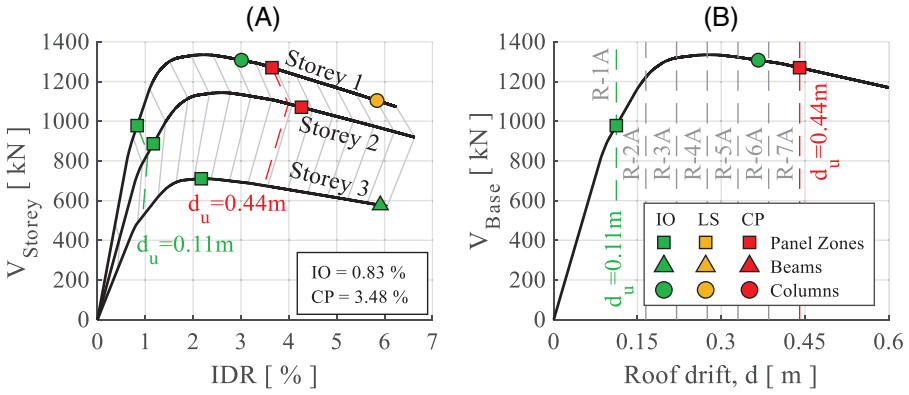

FIGURE 4 Pushover of the bare frame of case study structure A, including markers for the ASCE 41-17 performance levels. (A) Capacity curves for each storey in terms of IDR and storey shear. Grey lines represent 0.05 m drift intervals of the top storey; (B) Pushover curve for the structure

stiffness; (2) the Life Safety (LS) structural performance level, where the damaged structure retains a margin of safety against the onset of partial or total collapse; and (3) the Collapse Prevention (CP) structural performance level, where the damaged structure continues to support gravity loads but has no margin to withstand lateral loads to avoid collapse.[5,15]

Figure 4(A) shows the relationship between the IDR and the storey shear (V_{Storey}) during the pushover analysis of case study structure A; while Figure 4(B) shows the pushover curve in terms of the top storey (i.e., 3rd storey) drift (d) and base shear (V_{Base}). In addition, the figures indicate the steps at which the demands exceed the code-based acceptance criteria at each performance level and for each element typology. For case study structure A, the panel zones are the first elements to exceed the acceptance criteria in all structural performance levels. The IO is first reached by the panel zones at the 1st storey, for a top storey drift of 0.11 m (IDR of 0.83%, 1.05% and 0.94% for the first, second and third storeys, respectively). The LS and CP are reached simultaneously for a top storey drift of 0.44 m (IDR of 3.65%, 3.99% and 3.48%), as the panel zones deformation controls the capacity, and, according to the ASCE 41-17 regulations, their acceptance criteria are identical for LS and CP. It is noteworthy that the bottom storey columns have already exceeded the IO for this deformation value.

2.3 | Retrofitting design objectives and seismic demand

Seven retrofitting configurations are established in terms of target top storey drift (d_u). For this purpose, the properties of the retrofitting system are calibrated such that its maximum capacity is reached at the desired d_u value, as detailed in Section 2.4. These retrofitting configurations are equally distributed within two boundary design objectives: (1) the lower boundary (d_u = 0.11 m), in which the design objective is to protect the MRF from damage (i.e., all of the MRF elements remain below the IO) hence promoting the resilience of the structure (i.e., easy reparability of the structure through substitution of the BRBs); and the upper boundary (d_u = 0.44 m), that represents a design objective in which the MRF provides a larger relative contribution to the dual system capacity, thus allowing the development of a limited amount of damage in the existing elements (i.e., any of the MRF elements can overpass the IO, but must remain below the CP). The other five target top storey drift (d_u) values are defined to investigate intermediate situations, as it is summarised in Table 2 and illustrated in Figure 4(B).

TABLE 2 Target top storey drift (d_u) for the retrofitting of the case study structure A

Retrofitting scheme	R-1A	R-2A	R-3A	R-4A	R-5A	R-6A	R-7A
Target top storey drift, d_u [m]	0.11	0.165	0.22	0.275	0.33	0.385	0.44

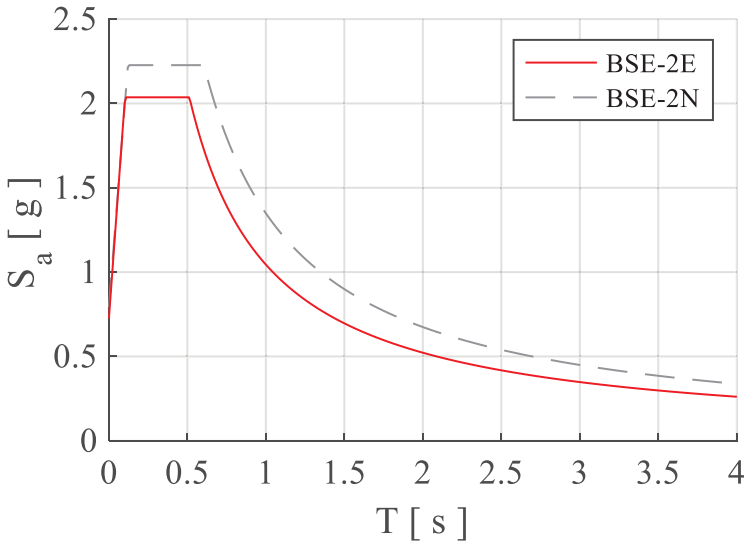

FIGURE 5 Site response spectra for Los Angeles, site Class D with 3% damping, as defined by ASCE 41-17

The design of all of the retrofitting schemes is carried out by pairing the damage state associated to the failure of the BRBs with the hazard associated to CP in the ASCE 41-17. The ASCE 41-17 acknowledges that the performance expected from retrofitted structures is not necessarily equivalent to the performance of newly built structures (15 §C2.2.1); thus, the return period of the hazard is established accordingly. For this purpose, the ASCE 41-17 proposes the Basic Performance Objective for Existing Buildings (BPOE), which, in the case of Risk Category II buildings (as the case study structures), pairs the CP to the BSE-2E hazard level, which is associated to a probability of exceedance of 5% in 50years (or 975 years mean return period).

Figure 5 shows the site response spectrum associated with the BSE-2E hazard level for Los Angeles, considering a site Class D and a 3% damping, as defined by ASCE 41-17. This response spectrum is characterised by $S_{XS} = 1.81$ g, $S_{X1} = 0.92$ g and $B_1 = 0.89$. In addition, Figure 5 shows the response spectrum associated with the hazard level required for new buildings (BSE-2N) for comparison purposes. The BSE-2N hazard is equivalent to the risk-targeted maximum considered earthquake (MCE_R) of the ASCE 7–16, which is defined by considering a uniform-risk approach rather than a uniform-hazard one and is related to a 1% probability of collapse in 50 years.

2.4 | Retrofitting design procedure

The design of the retrofitted structures considers a dual system configuration, in which the existing MRF and the BRBF work in parallel. The design procedure for the BRBs is similar to the approach used by previous authors[20] and relies on an equivalent SDoF approximation.[17] The main objectives of the design procedure are: (1) to produce a controlled increase of the base shear capacity of the system, i.e., the base shear of the dissipative system when added to the base shear of the bare frame; (2) to increase strength, stiffness, and energy dissipation capacity of the structure while maintaining a proportional response per storey. In particular, (2a) the strength of the BRBs is distributed among the storeys to produce the simultaneous yielding of the BRB devices hence maximising the energy dissipation capacity; and (2b) the stiffness and ductility of the devices are calibrated to allow the BRB device failure to occur about simultaneously at the target top storey drift (d_u). The design procedure is illustrated in Figure 6 and summarised as follows:

1. The pushover curve of the bare frame (Figure 4(B)) with the chosen target top storey drift (d_u) is bi-linearised into an elastic perfectly plastic system based on an equal energy approach allowing the definition of the yielding parameters (i.e., $F_{y\text{-}MRF}$, $d_{y\text{-}MRF}$).

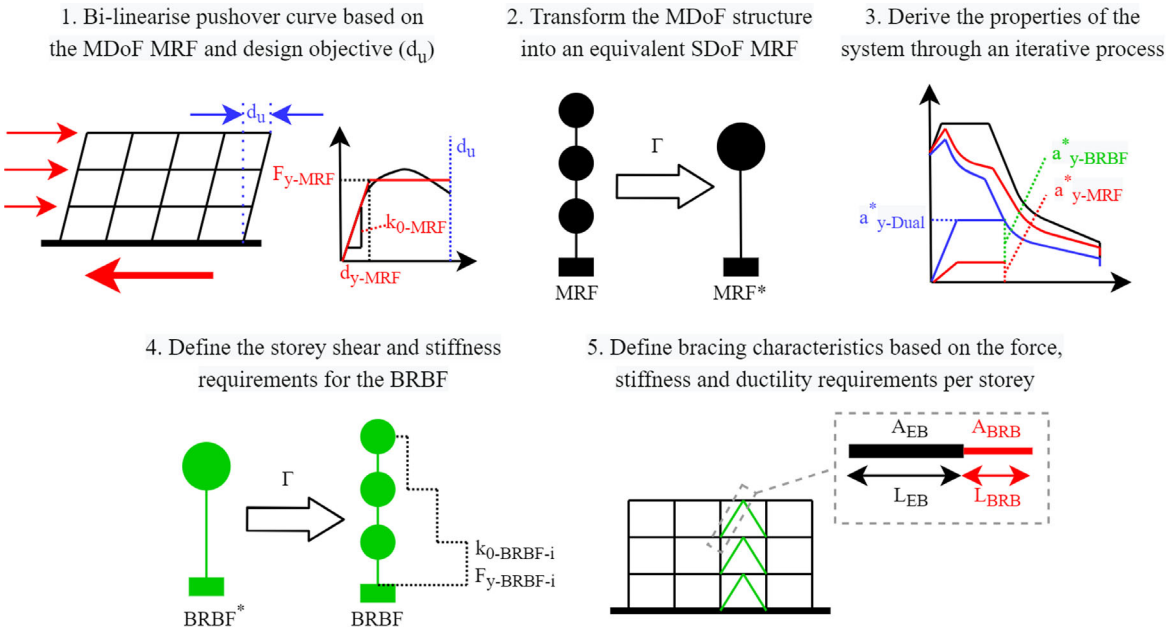

FIGURE 6 Design procedure for the retrofitting of the case study structures

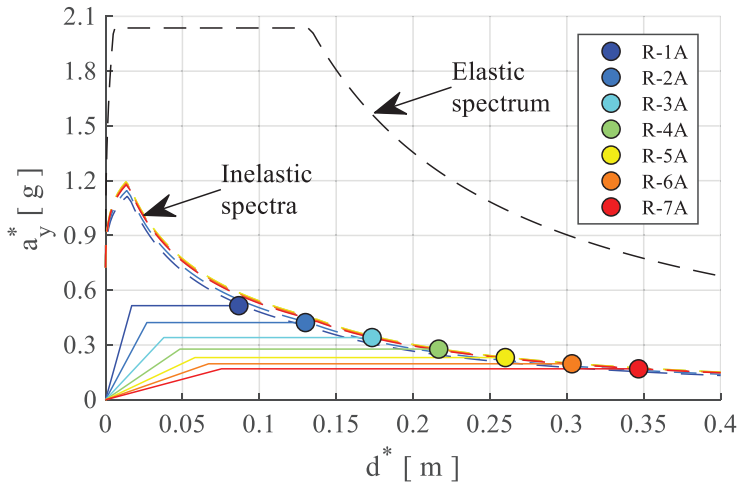

FIGURE 7 Capacity curves for the retrofitted (i.e., dual system) SDoF structures of case study structure A, elastic and inelastic demand response spectra (BSE-2E hazard level), and performance points in the ADRS plane

2. The pushover curve of the multi-degree of freedom system (MDoF) is transformed into an equivalent SDoF system (i.e., with parameters $F^*_{y\text{-}MRF}$, $d^*_{y\text{-}MRF}$, d^*_u) and compared with the inelastic response spectrum demand within the ADRS plane[17] (i.e., $a^*_{y\text{-}MRF} = F^*_{y\text{-}MRF}/m^*$ is compared with the seismic demand). As the inelastic response spectrum depends on the ductility of the dual system ($\mu_{Dual} = d_u/d_{y\text{-}Dual}$), which simultaneously depends on the capacity of the BRBF, the following iterative procedure is required:
   (a) assume an initial value for μ_{Dual};
   (b) define the corresponding inelastic response spectrum;
   (c) define the required capacity in the BRBF (i.e., $a^*_{y\text{-}BRBF} = F^*_{y\text{-}BRBF}/m^*$) by the comparison of the inelastic response spectrum demand and the capacity of the MRF;
   (d) calculate the initial stiffness of the BRBF ($k_{0\text{-}BRBF}$) based on the assumed design ductility of the BRBF (μ_{BRBF}). In the present study, μ_{BRBF} is assumed equal to 12.6 for all retrofitting schemes;
   (e) define the properties of the dual system (i.e., $k_{0\text{-}Dual}$, $a^*_{y\text{-}Dual}$, μ_{Dual}) by summing the contributions of the MRF and BRBF;
   (f) repeat steps (b) to (e) with the new μ_{Dual} until convergence is found.

Figure 7 shows the capacity curves for all the retrofitted SDoF structures of case study structure A and the demand response spectra in the ADRS plane.

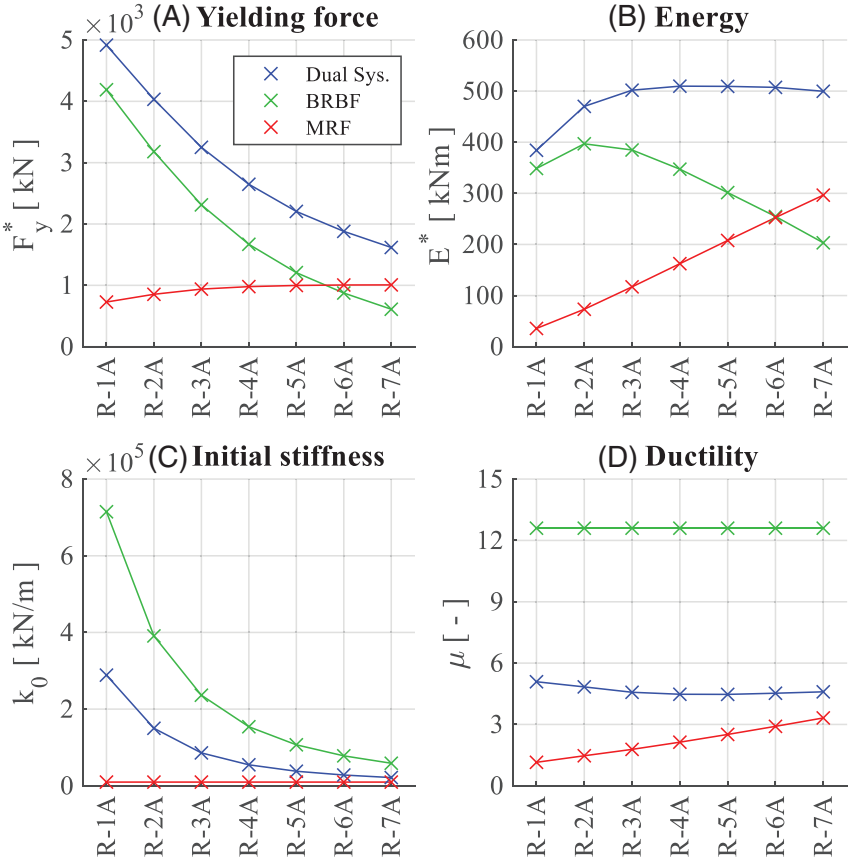

FIGURE 8 Main characteristics of the equivalent SDoF systems of case study structure A: (A) yielding force, F^*_y; (B) energy (area under the curve), E*; (C) initial stiffness, k_0; (D) ductility, μ

3. The characteristics of the BRBF are transformed back into a MDoF system. The horizontal yielding force and initial stiffness per storey ($F_{y\text{-}BRBF\text{-}i}$, $k_{0\text{-}BRBF\text{-}i}$) are calculated as follows:

$$F_{y-BRBF-i} = F^*_{y-BRBF}\Gamma\nu_i \qquad k_{0-BRBF-i} = \frac{\mu_{BRBF}F_{y-BRBF-1}}{d_u}\frac{\nu_i}{\Phi_i - \Phi_{i-1}} \tag{1}$$

where Γ is the modal participation factor, Φ_i is the mode shape factor, and ν_i is the storey shear shape factor defined as follows:

$$\nu_i = \sum_{n=i}^{3}\frac{m_n\Phi_n}{m_1\Phi_1} \tag{2}$$

4. Assuming the Maximum Ductility Capacity (MDC) for the BRB devices (i.e., $\mu_{BRB} = 20$ in the present study), the yielding resistance of the material for BRB devices ($f_{y,BRB} = 322$ MPa), and based on strength $F_{y\text{-}BRBF\text{-}i}$, and stiffness $k_{0\text{-}BRBF\text{-}i}$ of the dissipative braces, the properties of the components can be easily derived. The cross-sectional area of the BRB devices (A_{BRB}) is derived based on the force demand and number of braces per storey $F_{y\text{-}BRBF\text{-}i}$, while the length of each BRB device (L_{BRB}) is based on the plastic deformation required to achieve the target top storey drift, d_u. The properties of the EB (A_{EB}, L_{EB}) are derived to comply with the stiffness demand per storey $k_{0\text{-}BRBF\text{-}i}$, by considering a series arrangement of the components.[7]

Figure 8 shows a summary of the design parameters for the SDoF equivalent systems, including (A) the yielding force of the bilinear capacity curves, (B) the energy dissipation capacity (i.e., the area under the curves), (C) the initial stiffness and (D) the ductility. As a general rule, it is observed that the retrofitting schemes with lower target top storey drift (e.g., R-1A) are characterised by stiffer and stronger dual systems; nonetheless, the energy displaced is lower than in the retrofitting schemes with larger target top storey drifts (e.g., R-7A). As previously stated, the MDC of the BRB device is considered

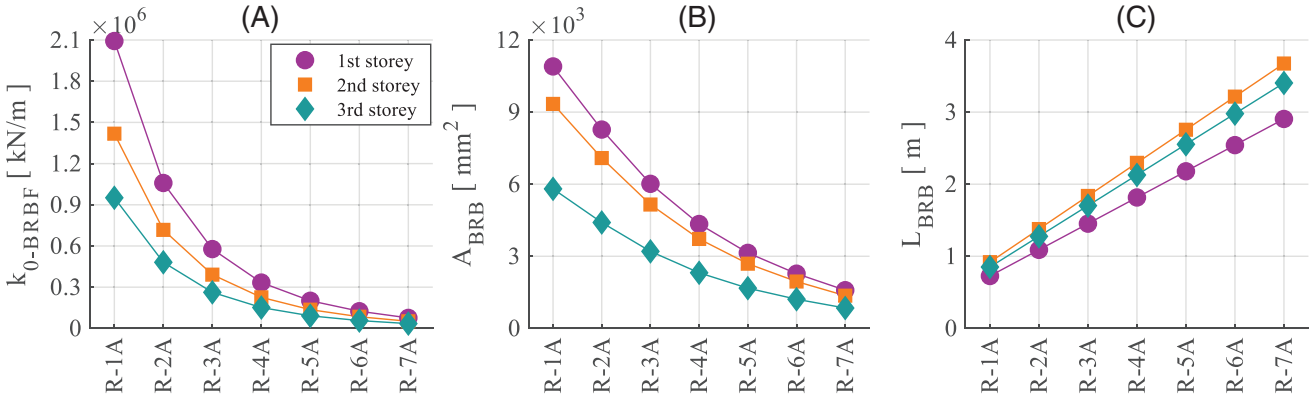

FIGURE 9 Bracing system characteristics of case study structure A: (A) BRBF stiffness per storey; (B) Cross-sectional area of BRB devices; (C) Length of BRB devices

to be $\mu_{BRB} = 20$, which is consistent with the values described in previous experimental work.[44] As a consequence of the design methodology, the design ductility for the entire BRBF is equal with the ductility of each individual BRB (i.e., BRB device plus the EB), which for this study is considered $\mu_{BRBF} = 12.6$. As a result, when combined with the MRF in a dual system configuration, the ductility of the entire system ranges from $\mu_{Dual} = 4.47$ (in R-5A) to 5.09 (in R-1A), as observed in Figure 8(D).

The design characteristics of the BRB devices for case study structure A are shown in Figure 9, including (A) the initial horizontal stiffness at each storey, (B) the cross-sectional area and (C) the lengths of the BRB devices. Although some of the retrofitting schemes result in dimensions that could become impractical, these extreme cases are included in the present study with the purpose of covering a large range of retrofitting design solutions within the boundaries delimited by the IO and the CP structural performance levels in the MRF. In addition, the storey strength and stiffness demands could be covered by including more BRBs per storey without significantly altering the response of the structure; yet these assumptions are out of the scope of the present work.

2.5 | Pushover analyses on case study structure A

For the definition of fragility relationships in the structures, this study considers three structural EDPs for the MRF, including the chord rotation in beams, the chord rotation in columns and the distortion in panel zones, as well as the ductility in BRB devices. The structural EDPs related to the MRF are evaluated by considering the acceptance criteria for the three structural performance levels outlined in the ASCE 41-17, previously summarised in Table 1. For the ductility in BRB devices, the MDC value considered is $\mu_{BRB} = 20$.

Figure 10 shows the relationship between the IDR and the storey shear (V_{Storey}) during the pushover analysis for all the retrofitted structures and the bare frame. In addition, the points at which any element of each type (e.g., BRBs, panel zones, columns and beams) exceeds the acceptance criteria for a given structural performance level at each storey are marked. As observed, the damage progression is consistent with the boundary design objectives: R-1A reaches the MDC in the BRBs before the panel zones (and other structural elements in the MRF) reach the IO structural performance level. On the other hand, R-7A reaches the MDC in the BRBs, closely followed by CP in the panel zones. The LS structural performance level does not appear in Figure 10 as the acceptance criteria for panel zones at the LS and CP are the same (i.e., $\Delta_p > 12\theta_y$).

In general, for all performance levels, the panel zones are the critical elements of the bare frame structure; however, in all retrofitted cases, the BRBs exceed the MDC before the MRF elements exceed the CP. It is also worth highlighting that, in accordance with the objectives of the retrofitting design methodology, all the BRBs at all storeys show similar ductility demand values, which allows them to exceed their capacity limits almost simultaneously during the pushover analyses. Moreover, no force-controlled capacity limits are exceeded, and no soft-storey mechanisms are observed in any of the cases.

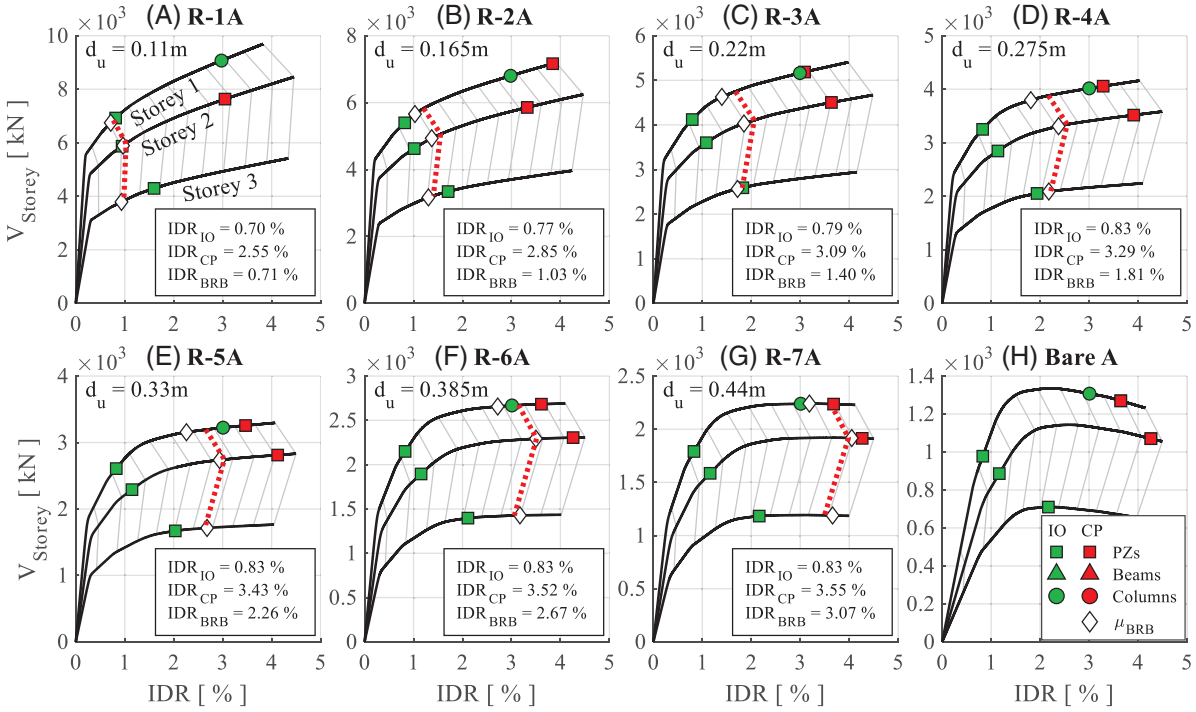

FIGURE 10 Capacity curves per storey with performance levels for the retrofitted structures (a to g) and the bare frame (h) of case study structure A. Grey lines represent 0.05 m top storey drift intervals, while red dotted lines represent the step at which the target top storey drift (d_u) value is reached. In addition, the minimum IDR is indicated, based on the first element in the MRF (IDR_{IO} and IDR_{CP}) to exceed the acceptance criteria for a given performance level and the first BRB to reach its MDC (IDR_{BRB})

3 | FRAGILITY AND RISK ASSESSMENT PROCEDURES AND APPLICATION TO CASE STUDY STRUCTURE A

The bare frame and retrofitted structures based on case study structure A are assessed through fragility and risk analyses allowing the comparisons in terms of structural damage, non-structural damage, residual storey drifts, and cumulative ductility in the BRB devices. The fragility relationships are defined through Incremental Dynamic Analyses (IDAs)[45] by considering code- and literature-defined limits for various performance levels. Each fragility curve relates an IM with the probability of exceeding the acceptance criteria associated with a given performance level. In addition, risk estimates allow the comparison among the retrofitted cases accounting for the variation in terms of capacity of the structures (i.e., fragility curves) and seismic demands (i.e., hazard curves) due to the variation of the fundamental period of vibration.

The fragility assessment is carried out by considering a set of 30 ground motion records selected from the PEER NGA-West2 database.[46] These ground motion records are selected by using the BSE-2E spectrum as a reference, considering a period range from $0.2T_{1\text{-min}}$ to $1.5T_{1\text{-max}}$ (i.e., from 0.1 to 2.82 s for case study structure A). This period range is based on the ranges often considered in literature (e.g., 47, 48), which are used to consider the contribution of higher modes and the possible elongation of the fundamental period. The selected ground motions for case study structure A are characterised by magnitudes from $M_w = 5.2$ to 7.36, and correspond to far-field records with a mean significant duration ($D_{5\text{-}95\%}$) of 18.59 s, and a mean rupture distance (R_{rup}) of 29.79 km. The spectra for the selected ground motions, normalised by the peak ground acceleration (PGA) in the design spectrum, are shown in Figure 11. Fragility curves are derived through an IDA procedure, using the spectral acceleration at the fundamental period of the structure, $S_a(T_1)$, as IM. The ground motions are scaled in order to match different values of $S_a(T_1)$, with smaller discretisation in lower values of intensity (every 0.02 g up to 0.1 g, and every 0.1 g onwards). The median scaling factors to match the IM associated with the MDC in BRBs (retrofitted structures) or the CP in the MRF (bare frame structures) range from 5.07 in R-1A to 7.31 in the bare frame of case study structure A.

Although a comparison between fragility curves allows drawing capacity-based comparisons, the change in the dynamic properties of the building also affects the demands to which the structure is subjected to. Therefore, a comprehensive comparison should consider the site-dependent demands in a risk-based approach. Thus, the local hazard information

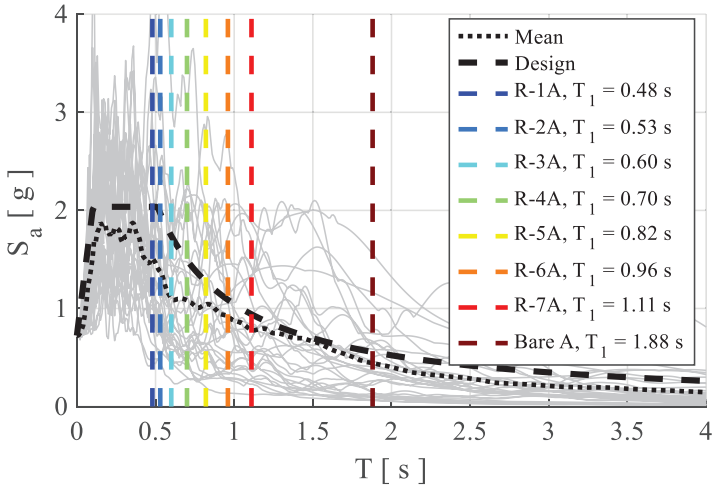

FIGURE 11 Response spectra corresponding to the 30 unscaled ground motion records used during the IDA for case study structure A, with 3% damping, normalised by the PGA in the design spectrum

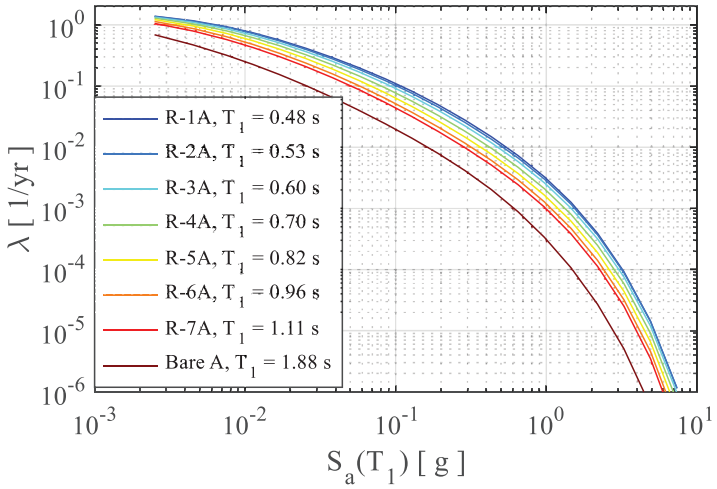

FIGURE 12 Hazard curves for Los Angeles, site Class D, by considering the fundamental periods of the bare and retrofitted schemes of case study structure A. The curves corresponding to the periods of interest are linearly interpolated from the λ for adjacent periods. Based on the hazard values obtained from the Unified Hazard Tool[49]

for Los Angeles is obtained through the USGS Unified Hazard Tool[49] by using the Conterminous US database (v4.2.0) and considering site Class D (V_{s30} = 259 m/s). The hazard curves corresponding to the fundamental period of the bare and retrofitted schemes of case study structure A are shown in Figure 12.

Thus, the annual probability of exceedance (P_{1Y}) is obtained through the convolution of the fragility and hazard curves, as follows:

$$P_{1Y} = \int_0^{IM_i=IM_{max}} P\left(EDP \geq AC_{PL} \,|IM = IM_i\right) \left(\frac{d\lambda\left(IM_i\right)}{d\left(IM_i\right)}\right) d\left(IM_i\right) \tag{3}$$

where λ represents the hazard's annual frequency of exceedance and AC_{PL} is the acceptance criteria (i.e., capacity limit) associated with a given performance level. The lifetime probability of exceedance (P_{50Y}), which corresponds to the probability of exceedance in T_N = 50 years, is obtained as follows:

$$P_{50Y} = P\left(EDP \geq AC_{PL} \,|50 \text{ years}\right) = 1 - \left(1 - P_{1Y}\right)^{T_N} \tag{4}$$

3.1 | Structural damage assessment

The local EDPs of the bare and retrofitted versions of case study structure A are recorded throughout the analyses, and their peak deformation demands are contrasted with the ASCE41-17 acceptance criteria for beams, columns and panel zones,

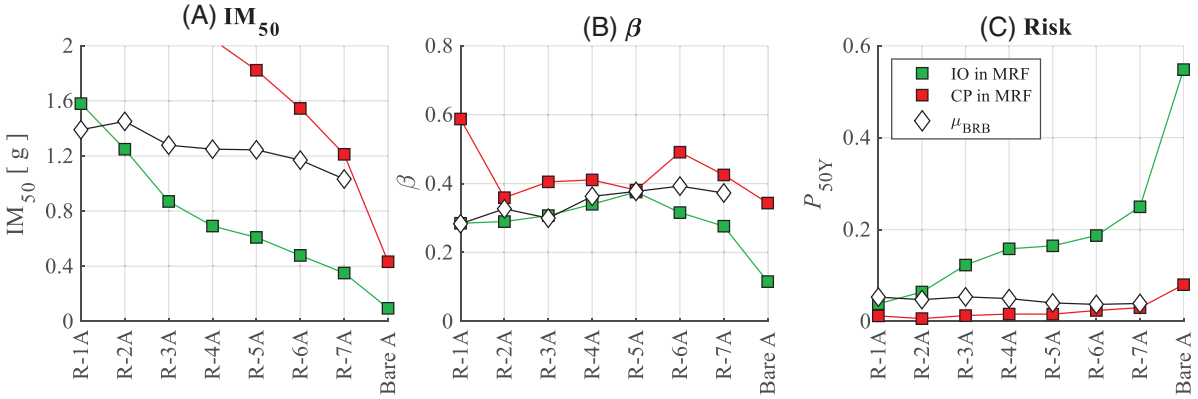

FIGURE 13 Structural fragility parameters and risk values for the bare frame and retrofitted schemes of case study structure A at all structural performance levels defined by ASCE 41-17

at all structural performance levels (IO, LS and CP). Similarly, the ductility demands on the BRB devices are contrasted to their MDC values. As shown in Figure 13(A), when considering the structural damage in the MRF, the median capacity (IM_{50}) of all the retrofitted structures is increased with respect to the bare frame for all performance levels. The IM_{50} for the MDC of the BRBs follows the same trend, as the stiffer frames exhibit the larger median capacity; nonetheless, the difference between the median capacity values for different retrofitting schemes is not as significant, with R-2A exhibiting the highest median capacity (1.45 g) and R-7A the lowest one (1.03 g).

When the comparison is performed in terms of risk, all of the retrofitted structures exhibit lower values of risk for the IO and CP structural performance levels than the bare frame, as shown in Figure 13(C). For the IO, the risk values are significantly reduced from the bare frame, with 0.55, to the most flexible retrofitted building (R-7A), which exhibits a risk value of 0.25. From there, the risk values continuously reduce to 0.04 at the stiffest structure (R-1A). In the case of the CP, this decreasing trend is also observed as the risk value of 0.08 in the bare frame is reduced to only 0.03 in the R-7A and 0.01 in R-1A. Nonetheless, all the CP risk values in the retrofitted structures are lower than their respective risk values for MDC in BRBs, thus become less relevant.

The risk values for the MDC remain fairly similar for all retrofitting schemes, which is consistent with the retrofitting design objectives. The risk values oscillate around 0.05 for R-1A to R-4A and slightly reduce to 0.04 for R-5A to R-7A. It is worth highlighting that the observed risk values for the IO in R-1A and for CP in R-7A are lower than the risk values corresponding to the MDC of the BRBs, which is consistent with the design objectives.

3.2 | Non-structural damage assessment

The non-structural assessment is made by considering damage in drift- and acceleration-sensitive components. For this purpose, the HAZUS MR4 Technical Manual[50] is used as a reference to establish the acceptance criteria for different non-structural damage state classifications (analogous to the performance levels in ASCE 41-17). In the case of drift-sensitive components, the manual makes use of IDR limits of 0.004, 0.008, 0.025 and 0.050 for the Slight (S), Moderate (M), Extensive (E) and Complete (C) damage state classifications, respectively. These values are considered the same for all kinds of structures regardless of the lateral resisting system typology (e.g., braced, MRF). As observed in Figure 14(A), the IM_{50} values for the IDR_{MAX} (i.e., the maximum-over-time IDR in all storeys) increase in larger retrofitting schemes, as it is directly dependent on the lateral stiffness. On the other hand, the risk values shown in Figure 14(C) follow the opposite tendency as the bare frame structure exhibits the largest risk values in all damage state classifications. Nonetheless, the risk reduction is more noticeable when lower damage states classifications are considered. It is noteworthy that the IDR_{MAX} limit values used by HAZUS MR4 are considerably large for the Extensive and Complete damage state classifications; thus, the non-structural drift values become irrelevant in most cases as they exceed the MDC risk values in which the total loss of the building is assumed.

In the case of the acceleration-sensitive components, the manual uses storey acceleration acceptance criteria that vary depending on the seismic design level of the structure. For comparison purposes, in this paper, the limits corresponding to moderate-code structures are used; thus, the storey acceleration limits are considered as 0.25, 0.5, 1.0 and 2.0 g for

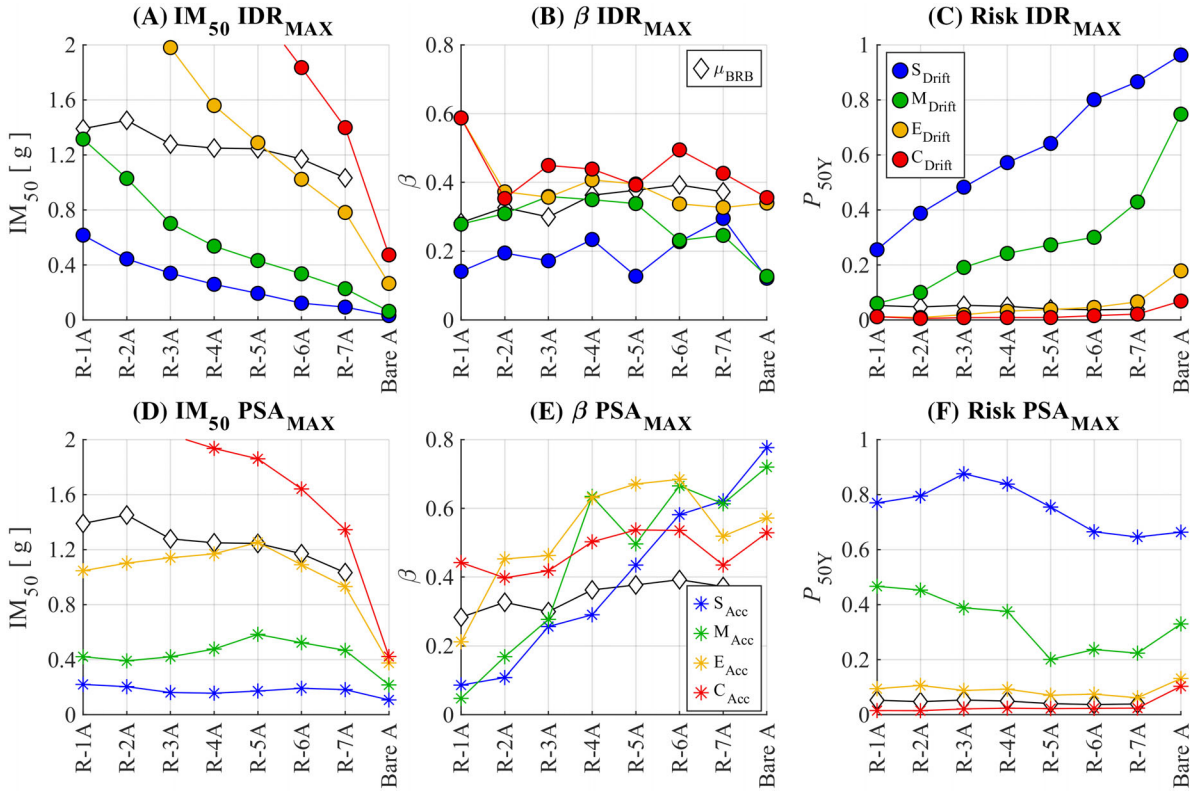

FIGURE 14 Non-structural fragility parameters and risk values for the bare frame and retrofitted schemes of case study structure A: (A) to (C) for the drift-sensitive components (measured through IDR_{MAX}); (D) to (F) for the acceleration-sensitive components (measured through PSA_{MAX})

the Slight (S), Moderate (M), Extensive (E) and Complete (C) damage state classifications, respectively. The maximum-over-time storey acceleration values (PSA_{MAX}) are recorded and compared to the acceptance criteria to derive fragility curves and risk values, as shown in Figure 14(D) to 14(F). As observed, the addition of a stiffer retrofitting scheme tends to increase the IM_{50} values for the PSA_{MAX}, which is consistent with the observations made by previous researchers (e.g., 51). However, the larger dispersion values (i.e., β in Figure 14(E)) and the higher demand values nullify the capacity gains and result in risk values that are similar among all structures (Figure 14(F)).

3.3 | Residual drift assessment

In addition to the structural and non-structural damage, the residual inter-storey drift ratio (IDR_{RES}) is a key EDP to characterise the performance of BRBFs, as the BRB devices are often associated with large residual drifts due to their low post-yielding stiffness.[25,52] According to previous studies,[53,54] IDR_{RES} values larger than 0.5% are associated with repairing costs that exceed the costs of replacing the structure. Figure 15 shows the fragility parameters and risk estimates for the IDR_{RES} when considering a 0.5% acceptance criterion. In all cases, the retrofitted structures increase their median capacity with respect to the bare frame structure while increasing their dispersion. The larger retrofitting schemes (short BRB devices with large cross-sections) are associated with higher IM_{50} values, as the residual deformation in the BRBs is proportional to their length. In fact, when considering the risk values, the R-1A to R-5A schemes exhibit lower or similar values than the risk of exceeding the MDC. Only in the cases of R-6A and R-7A, the risk of exceeding the $IDR_{RES} = 0.5\%$ is meaningfully larger than the risk of exceeding the MDC. It is important to highlight that the current study neglects the possible re-centring capacity that the MRF elastic strains could provide after the removal of the damaged BRB devices in the dual system (as they are intended to be fuse elements); thus, the observed residual drift risk values could be lower and repairability even more feasible.

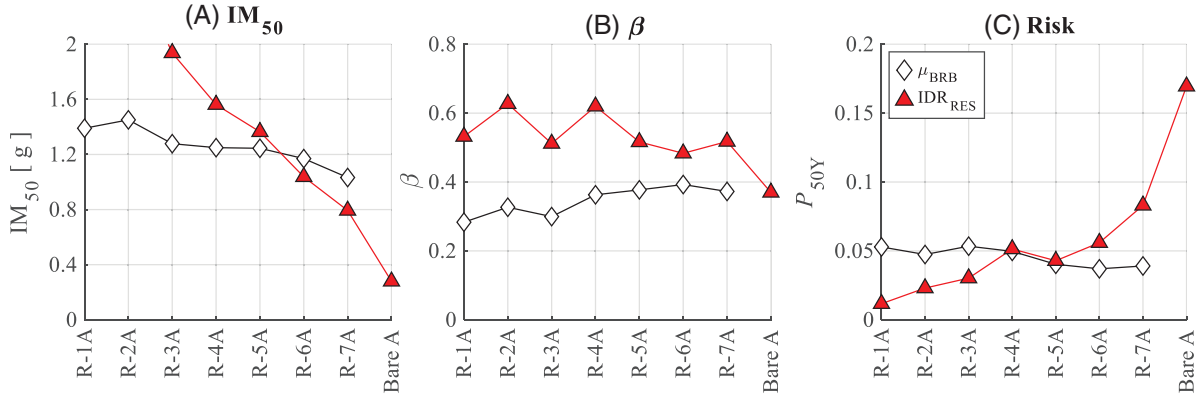

FIGURE 15 Fragility parameters and risk values for the bare frame and retrofitted schemes of case study structure A: residual inter-storey drift ratio (IDR_{RES})

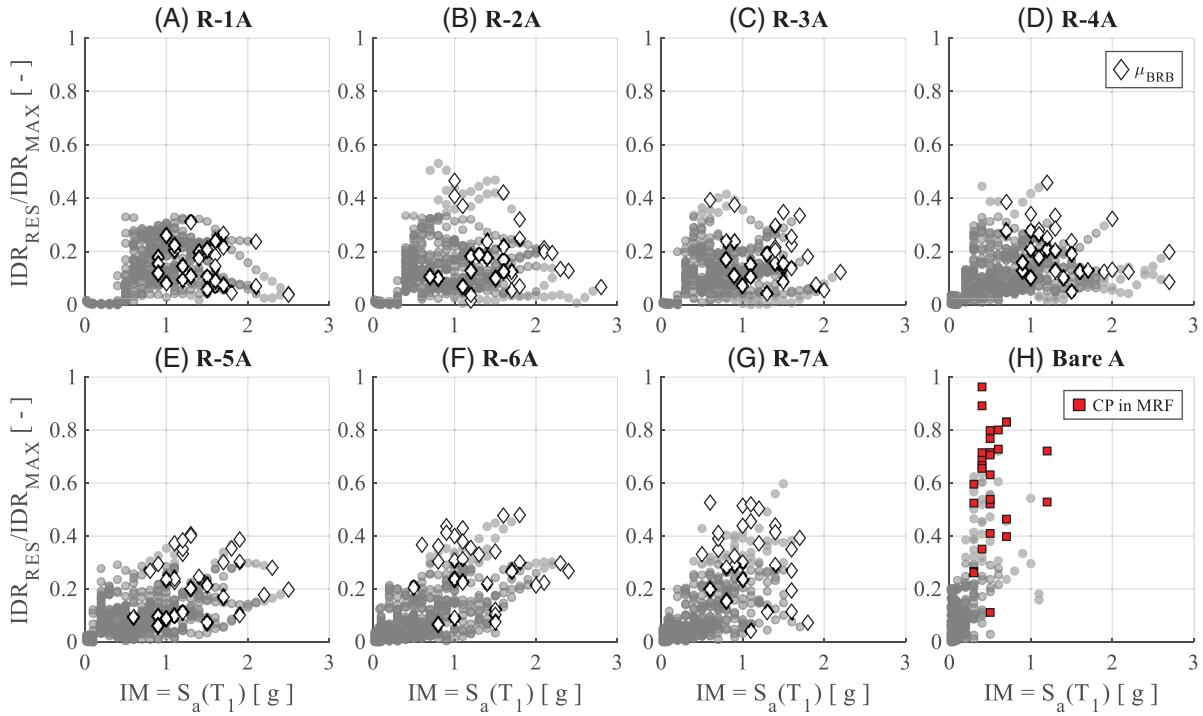

FIGURE 16 The ratio between residual inter-storey drift ratios (IDR_{RES}) and maximum inter-storey drift ratios (IDR_{MAX}) at each IM level, in the bare frame and retrofitted schemes of case study structure A

Figure 16 shows the ratio between the IDR_{RES} and the IDR_{MAX} for all IM values up to the point on which the BRBs reach their MDC (retrofitted frames) or the MRF reach the CP (bare frame). As observed, the ratio tends to slightly increase when the more flexible structures are considered. In general, the ratio oscillated around 0.40 for the retrofitted structures, while the bare frame exhibited significantly larger ratios.

3.4 | Hysteretic energy dissipation and cumulative ductility in BRB devices

The hysteretic energy dissipated through the plastic deformation in the structural elements is a useful parameter to synthetically represent the level of structural damage. For this purpose, Figure 17 shows a synthesised comparison between the mean hysteretic energy dissipated by the BRB devices and the MRF elements. The energy dissipation is directly recorded during the analysis by measuring hysteretic loops at each converging time-history analysis, then the mean of the recorded

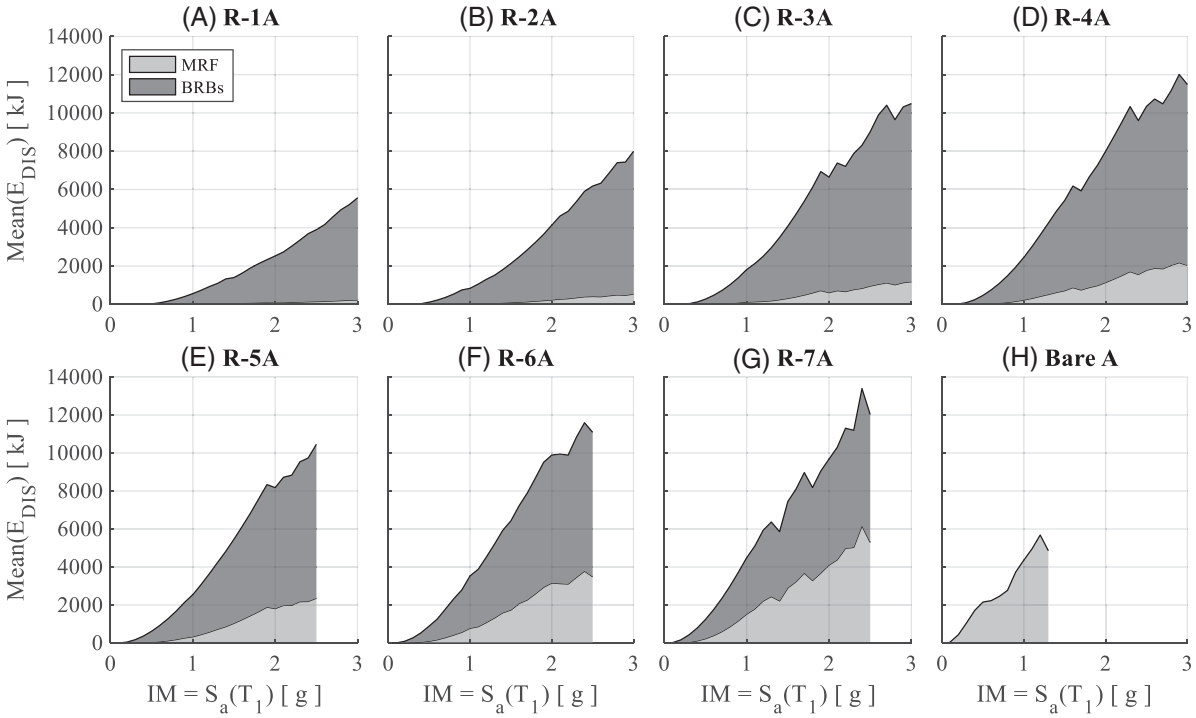

FIGURE 17 Comparison of the mean hysteretic energy dissipated by the BRBs and the MRF elements (panel zones, columns and beam plastic hinges) in the bare frame and retrofitted schemes of case study structure A

values, among all ground motions, is computed for each IM intensity. As observed, all the retrofitting schemes reduce the mean energy dissipated by the MRF elements, which suggest lower levels of damage in the MRF for all IM values. Although the energy dissipation alone is not necessarily an indicator of good performance, the comparison allows a synthetic comparison of the engagement level (i.e., damage) of the MRF with respect to the BRBs. As highlighted before, the concentration of damage in the BRBs and the reduction of damage in the MRF, increase the repairability of the structures, as the BRB devices can be easily replaced and the MRF are less likely to require repairments.

Some structural elements, such as the BRBs, are explicitly designed to contribute towards the improvement of the performance of the structure through their hysteretic energy dissipation capacity. Nonetheless, despite the apparent benefits of large energy dissipation in a structure, the use of the hysteretic energy as a sole parameter cannot be understood as a measure of structural performance, as the hysteretic energy dissipation is also a reflection of damage.

To measure the damage in the BRBs, the present study also considers the CDD imposed on the devices, as previous experimental studies[25] have shown their proclivity to develop low-cycle fatigue. The measurement of the CDD in a BRB becomes a straightforward task, as they can be measured directly from the time-history analyses. However, the definition of the capacity becomes a more challenging task, as the Cumulative Ductility Capacity (CDC) of a BRB is path-dependent (i.e., the demand history affects the CDC of the BRB devices).

To overcome this limitation, Andrews et al.[26] proposed a method based on a predictive model to estimate the CDC of BRB devices. This method is expressed in terms of dimensionless parameter ratios and calibrated on an extensive pool of previous experimental data, comprising 21 BRB device specimens that were cyclically loaded until they developed low-cycle fatigue. At each point of the load-paths, Andrews et al.[26] estimated the remaining CDC by considering the total capacity, experimentally measured at the end of the cyclic tests, minus the CDD up to the analysed point. The experimental results were fitted through a regression process to derive the remaining capacity (C_{REM}) model, which includes path- and non-path-dependent parameters, and is defined as follows:

$$C_{REM} = 2^{-21.2}\left(\frac{A_{BRB}}{(A_{BRB})_{max}}\right)^{0.425}\left(\frac{L_{BRB}}{(L_{BRB})_{max}}\right)^{0.044}(\varepsilon_{y-BRB})^{-3.45}\left(\frac{f_{u-BRB}}{f_{y-BRB}}\right)^{-1.46} - 152.9\left(\frac{\mu_{BRB-c}}{\mu_{BRB-ult}}\right) - 1.12\left(\frac{\mu_{BRB-max}}{\mu_{BRB-ult}}\right) \quad (5)$$

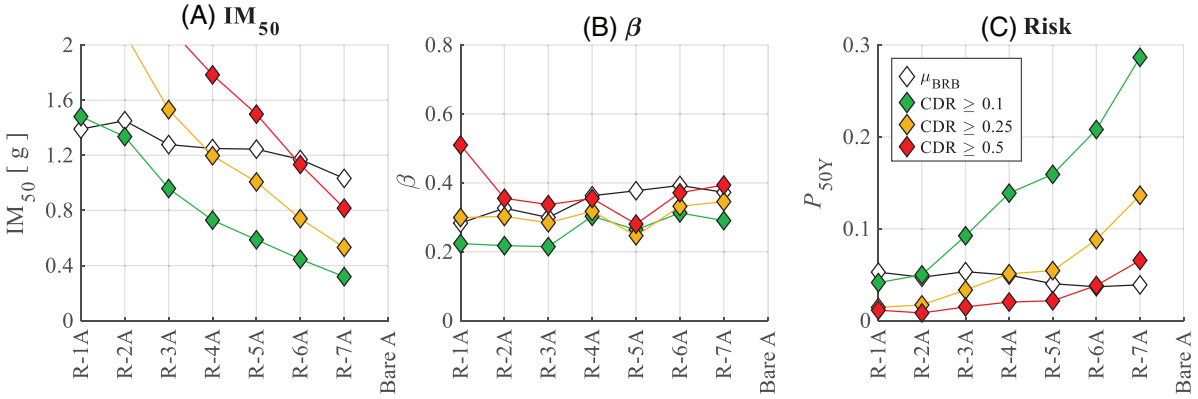

FIGURE 18 Fragility parameters and risk values for the bare frame and retrofitted schemes of case study structure A for cumulative ductility in BRB devices

where $\varepsilon_{y\text{-}BRB}$ is the yield strain of the BRB device core (e.g., $f_{y\text{-}BRB}/E_{BRB}$), $f_{y\text{-}BRB}$ and $f_{u\text{-}BRB}$ are the yielding and ultimate strength of the BRB core material, $\mu_{BRB\text{-}c}$ is the cumulative ductility at the analysed instant, equal to the sum of plastic deformation normalised by the deformation at yielding ($\Sigma\Delta_{p\text{-}BRB}/\Delta_{y\text{-}BRB}$), $\mu_{BRB\text{-}max}$ is the maximum ductility that the device underwent in its path-history since the undamaged state, $\mu_{BRB\text{-}ult}$ is the ratio between the ultimate tensile strain of the BRB device core $\varepsilon_{u\text{-}BRB}$ (normally considered as 0.35) and $\varepsilon_{y\text{-}BRB}$. Finally, $(A_{BRB})_{max}$ and $(L_{BRB})_{max}$ correspond to the maximum area and maximum length of the tested specimens, corresponding to 184.6 cm^2 and 472.1 cm, which were used as a reference for the fitting of the capacity model.

The first term in Equation (5) includes the non-path-dependend parameters, while the remaining two account for the path dependant. Therefore, when the remaining capacity is zero ($C_{REM} = 0$), the first term in Equation (5) is equal to the negative sum of the last two. Thus, an EDP related to the cumulative ductility is built by rearranging Equation (5) as follows:

$$CDR = \frac{152.9\left(\frac{\mu_{BRB-c}}{\mu_{BRB-ult}}\right) + 1.12\left(\frac{\mu_{BRB-max}}{\mu_{BRB-ult}}\right)}{2^{-21.2}\left(\frac{A_{BRB}}{(A_{BRB})_{max}}\right)^{0.425}\left(\frac{L_{BRB}}{(L_{BRB})_{max}}\right)^{0.044}\left(\varepsilon_{y-BRB}\right)^{-3.45}\left(\frac{f_{u-BRB}}{f_{y-BRB}}\right)^{-1.46}} \tag{6}$$

such that the cumulative ductility ratio (CDR) is equal to zero when the BRB is undamaged, and equal to one when the BRB has reached failure due to low-cycle fatigue. Three capacity limits are arbitrarily established for this EDP: CDR = 0.1, CDR = 0.25 and CDR = 0.5. Figure 18 shows the fragility parameters and risk estimates for all the retrofitted structures when considering the aforementioned limits for the cumulative ductility EDP. As observed, the stiffer structures exhibit larger IM_{50} values; nonetheless, β values remain almost constant for the same acceptance criteria. Thus, those structures with more flexible retrofitting schemes tend to exhibit higher risk values. Nonetheless, when compared with the risk of exceeding the MDC, none of the retrofitted schemes exceeds the 0.5 capacity limit, except for R-7A.

It is worth highlighting that the current observations do not disregard the possibility of low-cycle fatigue failure in any of the schemes, as the present study only considers the CDD corresponding to a single ground motion and disregards the cumulative damage due to multiple sequential ground motions. Nevertheless, the present values allow drawing general comparisons on the effects of cumulative ductility on the different retrofitting options.

4 | ASSESSMENT OF CASE STUDY STRUCTURE B

Case study structure B is subjected to the retrofitting and assessment procedures described in the previous Sections. This building is representative of an existing mid-rise steel MRF structure (6 storeys). The building is based on a modified version of a mid-rise, pre-Northridge steel MRF designed within the SAC Steel Project.[31] The details of case study structure B are shown in Figure 19.

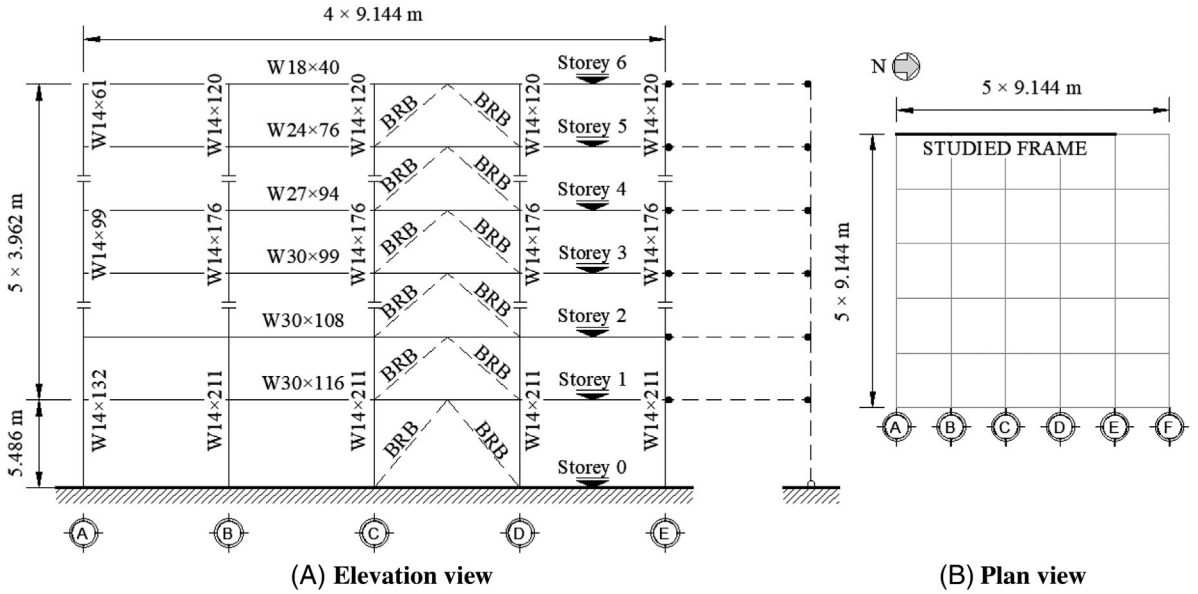

FIGURE 19 Case study structure B (representative of an existing mid-rise steel MRF) (A) elevation view, (B) plan view

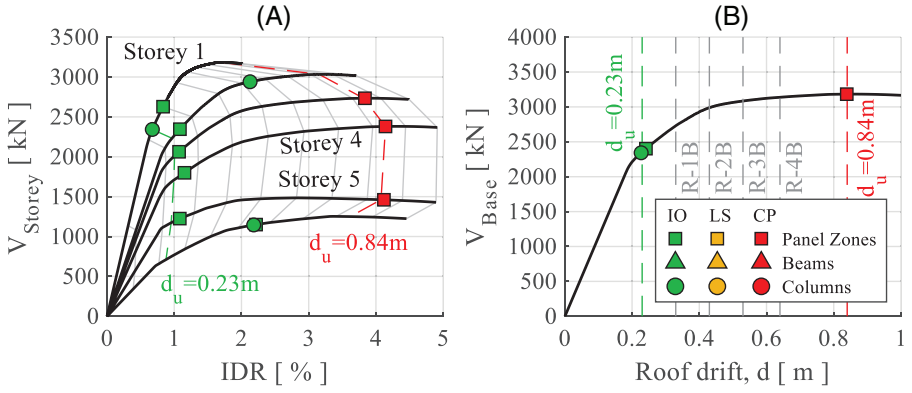

FIGURE 20 Pushover of the bare frame of case study structure B, including markers for the ASCE 41-17 performance levels. (A) Capacity curves for each storey in terms of IDR and storey shear. Grey lines represent 0.10 m drift intervals of the top storey; (B) Pushover curve for the structure

4.1 | Characteristics of the structure and retrofitting design

The material characteristics of the case study structure presented in this section match the characteristics of case study structure A, and the OpenSees numerical models are built by following the same assumptions and by utilising the same material constitutive models shown in Figure 2. The pushover of the bare frames in case study structure B is shown in Figure 20. In addition, markers are placed on the steps at which the acceptance criteria for each element typology are exceeded in all structural performance levels (i.e., IO, LS and CP). As observed, similarly to case study structure A, the panel zones in case study structure B are the most critical elements in their assessment for the LS and CP (which are exceeded simultaneously as the acceptance criteria is the same). Nonetheless, the IO is first exceeded by the columns in the base, closely followed by the panel zones.

Four target top storey drift (d_u) values are established for the retrofitting of case study structure B, all of them within the IO and CP boundaries for the MRF, as detailed in Figure 20 and Table 3. The retrofitting scheme design is carried out by following the procedures detailed in previous sections, and by considering the same site conditions and design assumptions. The main characteristics of the bracing systems are summarised in Figure 21.

TABLE 3 Design objectives in terms of target top storey drift (d_u) for the retrofitting of the case study structure B

Retrofitting scheme	R-1B	R-2B	R-3B	R-4B
Target top storey drift, d_u [m]	0.33	0.43	0.53	0.64

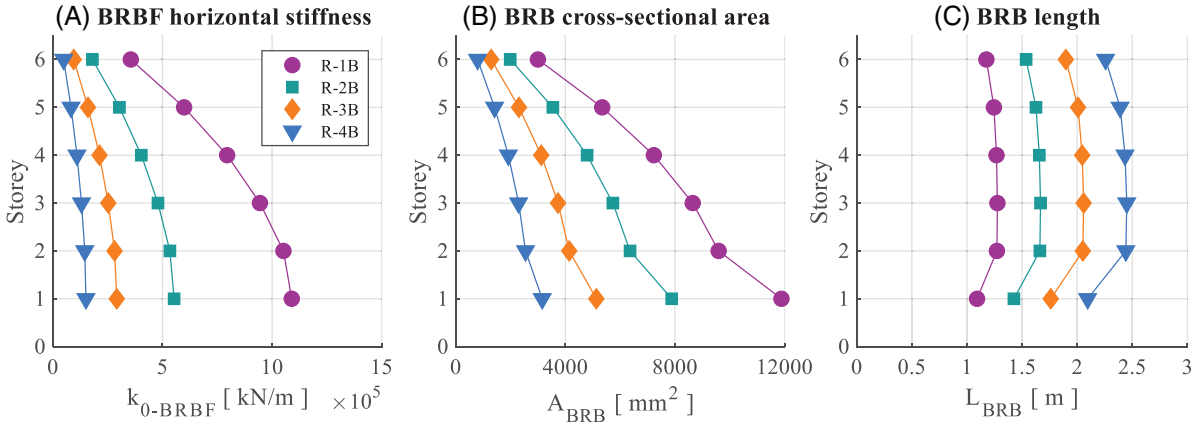

FIGURE 21 Bracing system characteristics for case study structure B

4.2 | Risk assessment o case study structures B

Similar to case study structure A, the bare and retrofitted versions of the case study structure B are assessed through IDAs by considering 30 ground motion sequences. Nonetheless, some of the selected ground motion records differ as they are chosen to match the site's design spectrum at different periods of interest ranges (i.e., the $0.2T_{1\text{-min}}$ to $1.5T_{1\text{-max}}$ are different for each case study structure). The fundamental period of the bare frame in case study structure B is 2.38 s, while the period of the retrofitted structures are 0.91, 1.04, 1.22 and 1.45 s for R-1B, R-2B, R-3B and R-4B, respectively.

Figure 22 shows the outcome of the risk assessment for both case study structures and offers a comparison of the results to evaluate the generality of the previously discussed outcomes. Similarly to case study structure A, the retrofitting with BRBs allows reducing the structural damage in the MRF elements, both in the IO and CP structural performance levels of case study structure B. As observed, the risk of exceeding the CP in the MRF of case study structure B is reduced from 0.08 in the bare frame to 0.03 in R-4B and 0.01 in R-1B to R-3B. Moreover, all of these risk values result lower than the risk of overpassing the MDC in the BRBs, which corresponds to 0.06 in R-1B and R-4B and to 0.04 in R-2B and R-3B. The decrease from the bare frame to the retrofitted structure is even more significant for the IO, as the risk values reduce from 0.58 in the bare frame to 0.10, 0.09, 0.10 and 0.19 for the R-1B, R-2B, R-3B and R-4B, respectively. In both case study structures, the addition of BRBs reduce the structural damage observed in the MRF elements, at all performance levels. In particular, larger cross-sectional areas in BRBs result more efficient as the structural damage in the MRF is proportional to the stiffness of the structure. Despite the increase of axial force demands in columns, no force-controlled failures are observed.

In the case of the risk of damage to non-structural components (second and third rows of Figure 22), the same trends are observed in both case study structures. When considering the drift-sensitive components, the retrofitting schemes with larger BRB cross-sections exhibit lower values of risk, as a direct result of the increase of lateral stiffness. Nonetheless, in the case of case study structure B, the performance gain in-between R-3B to R-2B and R-1B is negligible. In the case of the acceleration-sensitive components, no meaningful risk reduction is observed in case study structure A with respect to the bare frame, nonetheless, for case study structure B, the risk values are significantly reduced in the medium retrofitting schemes, particularly in R-3B, in which the risk values of 0.45, 0.11 and 0.07 in the bare frame, are reduced to 0.17, 0.04 and 0.01 for the Moderate (M), Extensive (E) and Complete (C) damage state classifications.

When comparing the structures in terms of residual drifts, the same pattern is observed in both case study buildings, as the bare frame structures exhibit the largest probability of exceeding the residual drift acceptance criteria, while the stiffest retrofitting schemes are less likely to exceed it. In most retrofitting cases, the risk of exceeding the residual drift limit of 0.5% is lower than the risk of exceeding the MDC in the BRBs. Finally, the CDR in all case study structures follows

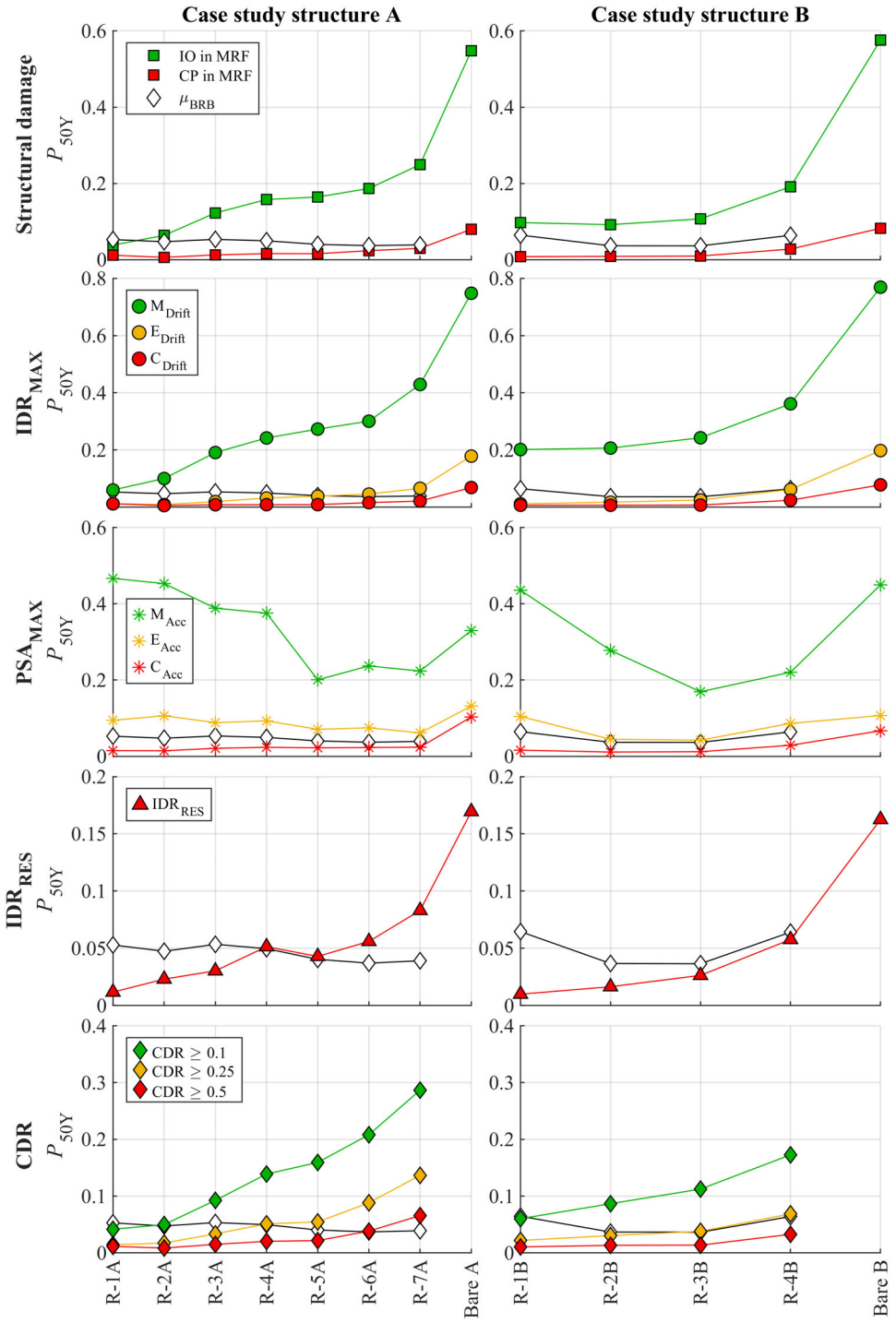

FIGURE 22 Risk values for all case study structures and all considered EDPs

the same pattern, as the most flexible BRBs are more likely to exceed the considered ratios. Nonetheless, none of the cases exhibit a meaningful probability of exceeding 0.5 times the predicted CDR after a single ground motion.

5 | CONCLUSION

The present study evaluated the seismic performance of two case study Moment Resisting Frame (MRF) structures when retrofitted by means of Buckling Restrained Braces (BRBs) and evaluated the influence of some relevant design parameters.

These case study structures are representative of existing low- and mid-rise steel MRFs. Several retrofitting schemes were proposed for each case study structure and designed by considering large seismic demands. The retrofitting schemes are designed at various top storey drift (d_u) objectives, and delimited by two boundary limits: (1) the maximum top storey drift permitted to avoid the MRF elements to exceed the acceptance criteria in the Immediate Occupancy (IO) structural performance level; and (2) the maximum top storey drift permitted to avoid the MRF elements to reach the Collapse Prevention (CP) structural performance level. The bare frames and retrofitted structures were assessed and compared by considering their structural and non-structural performance and their ability to avoid large residual drifts and avoid low-cycle fatigue in the BRB devices as a result of Cumulative Ductility Demand (CDD). The main conclusions can be summarised as:

- All of the retrofitting schemes in both case study structures are capable of reducing the damage to structural components in the MRF, as the stiffness increase reduce the deformation demands imposed on beams, columns and panel zones. On these case study structures, the risk of exceeding the Maximum Ductility Capacity (MDC) in the BRBs is larger than the risk of exceeding the CP in the MRF elements. Moreover, the risk of exceeding the MDC in any retrofitting scheme is lower than the risk of exceeding the CP in the bare frame, which highlights the efficiency of the retrofitting schemes in improving the performance of the case study structures.
- Although stiffer retrofitting options often exhibit higher median capacity values (IM_{50}) than the more flexible schemes, the change in their fundamental period increases the demands attraction, effectively nullifying performance increases as a result of the spectrum-consistent design approach used in this paper. When comparing the risk of exceeding the MDC among retrofitting schemes, the R-5A, R-6A and R-7A retrofitting schemes exhibit marginally lower values of risk (around 0.04) than the stiffer options (around 0.05), while R-2B and R-3B exhibit lower values of risk (0.04) than R-1B and R-4B (0.06).
- In all case study structures, the stiffest schemes provide the lowest risk values against damage of non-structural drift-sensitive components, as the damage in this component is given as a function of the maximum inter-storey drift ratio (IDR_{MAX}). On the other hand, none of the retrofitting schemes in case study structure A significantly reduced the risk of damage in acceleration-sensitive non-structural components. Nonetheless, this was not observed on the mid-rise case study structure B, as the risk values are consistently lower in the medium retrofitting schemes (e.g., R-3B) with respect to other schemes and the bare frame itself.
- When considering a residual inter-storey drift ratio (IDR_{RES}) limit of 0.5%, all of the retrofitting cases exhibit a significant risk reduction with respect to their bare frame structures. Moreover, most of the stiffer structures exhibited risk values that are lower or similar to the structural collapse risk.
- None of the retrofitting schemes resulted in low-cycle fatigue failure in BRBs after a single ground motion; nonetheless, it is observed that the more flexible retrofitting schemes make use of larger amounts of the available cumulative ductility. Thus, in ground motion sequences scenarios, these retrofitting schemes are more likely to develop low-cycle fatigue failure before the stiffer cases. In addition, these schemes allow larger amounts of damage (i.e., hysteretic energy dissipation) in the existing MRF structure, therefore, increasing its repairing costs and downtime.

Future research on this topic could be benefited from including cost analyses and ground motion sequences. These aspects allow enhancing the discussion, including the initial cost of the retrofitting schemes, the cost of replacing the BRB devices after a strong ground motion (or after large values of CDD) and the cost of repairing the damage in the MRF during the structuret's life span.

ACKNOWLEDGEMENTS

This research was partially funded by Consejo Nacional de Ciencia y Tecnología (Grant No. CONACYT-FiiDEM2018-000013-01EXTF-00148). Any opinions, findings, and conclusions or recommendations expressed in this paper are those of the authors and do not necessarily reflect the views of the funding agencies.

DATA AVAILABILITY STATEMENT

Data available on reasonable request to corresponding author.

ORCID

Fernando Gutiérrez-Urzúa https://orcid.org/0000-0002-3392-5312
Fabio Freddi https://orcid.org/0000-0003-2048-1166

REFERENCES

1. Federal Emergency Management Agency, State of the Art Report on Past Performance of Steel Moment-Frame Buildings in Earthquakes, FEMA 355E. (2000).
2. Di Sarno L, Paolacci F, Sextos AG. Seismic performance assessment of existing steel buildings: a case study. *Key Eng Mater*. 2018;763:1067-1076. doi:10.4028/www.scientific.net/KEM.763.1067
3. Di Sarno L, Freddi F, D'Aniello M, et al. Assessment of existing steel frames: numerical study, pseudo-dynamic testing and influence of masonry infills. *J Constr Steel Res*. 2021;185:106873. doi:10.1016/j.jcsr.2021.106873
4. American Institute of Steel Construction, Seismic Provisions for Structural Steel Buildings, ANSI/AISC 341-16, ANSI/AISC 341-16. (2016).
5. Gutiérrez-Urzúa F, Freddi F, Di Sarno L. Comparative analysis of code-based approaches for seismic assessment of existing steel moment resisting frames. *J Constr Steel Res*. 2021;181:106589. doi:10.1016/j.jcsr.2021.106589
6. Güneyisi EM. Seismic reliability of steel moment resisting framed buildings retrofitted with buckling restrained braces. *Earthq Eng Struct Dyn*. 2012;41:853-874. doi:10.1002/eqe.1161
7. Freddi F, Tubaldi E, Ragni L, Dall'Asta A. Probabilistic performance assessment of low-ductility reinforced concrete frames retrofitted with dissipative braces. *Earthq Eng Struct Dyn*. 2013;42:993-1011. doi:10.1002/eqe.2255
8. Almeida A, Ferreira R, Proença JM, Gago AS. Seismic retrofit of RC building structures with Buckling Restrained Braces. *Eng Struct*. 2017;130:14-22. doi:10.1016/j.engstruct.2016.09.036
9. Castaldo P, Tubaldi E, Selvi F, Gioiella L. Seismic performance of an existing RC structure retrofitted with buckling restrained braces. *J Build Eng*. 2021;33:101688. doi:10.1016/j.jobe.2020.101688
10. Della Corte G, D'Aniello M, Landolfo R. Field Testing of All-Steel Buckling-Restrained Braces Applied to a Damaged Reinforced Concrete Building. *J Struct Eng*. 2015;141:1-11. doi:10.1061/(asce)st.1943-541x.0001080
11. Xie Q. State of the art of buckling-restrained braces in Asia. *J Constr Steel Res*. 2005;61:727-748. doi:10.1016/j.jcsr.2004.11.005
12. Freddi F, Galasso C, Cremen G, et al. Innovations in earthquake risk reduction for resilience: recent advances and challenges. *Int J Disaster Risk Reduct*. 2021;60:102267. doi:10.1016/j.ijdrr.2021.102267
13. Tremblay R, Poncet L, Bolduc P, Neville R, DeVall R. Testing and design of buckling restrained braces for canadian application, in: 13th World Conf. Earthq. Eng., Vancouver, Canada, 2004.
14. Zona A, Dall'Asta A. Elastoplastic model for steel buckling-restrained braces. *J Constr Steel Res*. 2012;68:118-125. doi:10.1016/j.jcsr.2011.07.017
15. American Society of Civil Engineers. Seismic Evaluation and Retrofit of Existing Buildings, ASCE/SEI 41-17. 2017. doi:10.1061/9780784414859
16. American Society of Civil Engineers. Minimum Design Loads and Associated Criteria for Buildings and Other Structures, ASCE/SEI 7–16. 2017. doi:10.1061/9780784414248
17. Fajfar P. A Nonlinear Analysis Method for Performance-Based Seismic Design. *Earthq Spectra*. 2000;16:573-592. doi:10.1193/1.1586128
18. European Committee for Standardization (CEN). Eurocode 8: Design of structures for earthquake resistance - Part 1: General rules, seismic actions and rules for buildings, EN 1998-1. 2004.
19. Maley TJ, Sullivan TJ, Corte GDella, Development of a displacement-based design method for steel dual systems with buckling-restrained braces and moment-resisting frames. 2010. doi:10.1080/13632461003651687
20. Ragni L, Zona A, Dall'Asta A. Analytical expressions for preliminary design of dissipative bracing systems in steel frames. *J Constr Steel Res*. 2011;67:102-113. doi:10.1016/j.jcsr.2010.07.006
21. Di Cesare A, Ponzo FC. Seismic Retrofit of Reinforced Concrete Frame Buildings with Hysteretic Bracing Systems: design Procedure and Behaviour Factor. *Shock Vib*. 2017:2017. doi:10.1155/2017/2639361
22. Kalapodis NA, Muho EV, Beskos DE. Seismic design of plane steel MRFS, EBFS and BRBFS by improved direct displacement-based design method. *Soil Dyn Earthq Eng*. 2022;153:107111. doi:10.1016/j.soildyn.2021.107111
23. Freddi F, Tubaldi E, Zona A, Dall'Asta A. Seismic performance of dual systems coupling moment-resisting and buckling-restrained braced frames. *Earthq Eng Struct Dyn*. 2021;50:329-353. doi:10.1002/eqe.3332
24. Erochko J, Christopoulos C, Tremblay R, Choi H. Residual Drift Response of SMRFs and BRB Frames in Steel Buildings Designed according to ASCE 7-05. *J Struct Eng*. 2011;137:589-599. doi:10.1061/(asce)st.1943-541x.0000296
25. Takeuchi T, Miyazaki K, Ida M, Yamada S, Suzuki K. Estimation of Cumulative Deformation Capacity for Buckling Restrained Braces Placed in Frames. *J Struct Eng*. 2008;134:822-831. doi:10.1061/(ASCE)0733-9445(2008)134:5(822)
26. Andrews BM, Fahnestock LA, Song J. Ductility capacity models for buckling-restrained braces. *J Constr Steel Res*. 2009;65:1712-1720. doi:10.1016/j.jcsr.2009.02.007
27. Hoveidae N, Radpour S. Performance evaluation of buckling-restrained braced frames under repeated earthquakes. *Bull Earthq Eng*. 2021;19:241-262. doi:10.1007/s10518-020-00983-0
28. Freddi F, Padgett JE, Dall'Asta A. Probabilistic seismic demand modeling of local level response parameters of an RC frame. *Bull Earthq Eng*. 2017;15:1-23. doi:10.1007/s10518-016-9948-x
29. Ghowsi AF, Sahoo DR. Seismic performance of buckling-restrained braced frames with varying beam-column connections. *Int J Steel Struct*. 2013;13:607-621. doi:10.1007/s13296-013-4003-0
30. Freddi F, Ghosh J, Kotoky N, Raghunandan M. Device uncertainty propagation in low-ductility RC frames retrofitted with BRBs for seismic risk mitigation. *Earthq Eng Struct Dyn*. 2021:3456. doi:10.1002/eqe.3456
31. Gupta A, Krawinkler H. Behavior of Ductile SMRFs at Various Seismic Hazard Levels. *J Struct Eng*. 2000;126:98-107. doi:10.1061/(ASCE)0733-9445(2000)126:1(98)

32. National building code, Building Officials and Code Administrators International Inc., 1993.
33. McKenna F, Fenves GL, Scott MH. Open system for earthquake engineering simulation (OpenSees), 2000.
34. Lignos DG, Krawinkler H. Deterioration modeling of steel components in support of collapse prediction of steel moment frames under earthquake loading. *J Struct Eng*. 2011;137:1291-1302. doi:10.1061/(ASCE)ST.1943-541X.0000376
35. Zareian F, Medina RA. A practical method for proper modeling of structural damping in inelastic plane structural systems. *Comput Struct*. 2010;88:45-53. doi:10.1016/j.compstruc.2009.08.001
36. Castro JM, Elghazouli AY, Izzuddin BA. Modelling of the panel zone in steel and composite moment frames. *Eng Struct*. 2005;27:129-144. doi:10.1016/j.engstruct.2004.09.008
37. Falborski T, Hassan AS, Kanvinde AM. Column base fixity in steel moment frames: observations from instrumented buildings. *J Constr Steel Res*. 2020;168:105993. doi:10.1016/j.jcsr.2020.105993
38. Ibarra LF, Medina RA, Krawinkler H. Hysteretic models that incorporate strength and stiffness deterioration. *Earthq Eng Struct Dyn*. 2005;34:1489-1511. doi:10.1002/eqe.495
39. MacRae GA, Kimura Y, Roeder C. Effect of Column Stiffness on Braced Frame Seismic Behavior. *J Struct Eng*. 2004;130:381-391. doi:10.1061/(ASCE)0733-9445(2004)130:3(381)
40. Elkady A, Lignos DG. Effect of gravity framing on the overstrength and collapse capacity of steel frame buildings with perimeter special moment frames. *Earthq Eng Struct Dyn*. 2015;44:1289-1307. doi:10.1002/eqe.2519
41. Foutch DA, Yun SY. Modeling of steel moment frames for seismic loads. *J Constr Steel Res*. 2002;58:529-564. doi:10.1016/S0143-974X(01)00078-5
42. Kanvinde AM, Grilli DA, Zareian F. Rotational stiffness of exposed column base connections: experiments and analytical models. *J Struct Eng*. 2012;138:549-560. doi:10.1061/(ASCE)ST.1943-541X.0000495
43. Fisher JM, Kloiber LA. Base Plate and Anchor Rod Design. *AISC Steel Des Guid*. 2006;1:73.
44. Fahnestock LA, Sause R, Ricles JM. Seismic response and performance of buckling-restrained braced frames. *J Struct Eng*. 2007;133:1195-1204. doi:10.1061/(asce)0733-9445(2007)133:9(1195)
45. Vamvatsikos D, Cornell CA. Incremental dynamic analysis. *Earthq Eng Struct Dyn*. 2002;31:491-514. doi:10.1002/eqe.141
46. Bozorgnia Y, Abrahamson NA, Al Atik L, et al. NGA-West2 research project. *Earthq Spectra*. 2014;30:973-987. doi:10.1193/072113EQS209M
47. Song B, Galasso C, Kanvinde A. Advancing fracture fragility assessment of pre-Northridge welded column splices. *Earthq Eng Struct Dyn*. 2020;49:132-154. doi:10.1002/eqe.3228
48. Aljawhari K, Gentile R, Freddi F, Galasso C. Effects of ground-motion sequences on fragility and vulnerability of case-study reinforced concrete frames. *Bull Earthq Eng under rev*. 2020:1-21. doi:10.1007/s10518-020-01006-8
49. United States Geological Survey (USGS). Unified hazard tool, 2021. https://earthquake.usgs.gov/hazards/interactive/(accessed May 24, 2021)
50. Federal Emergency Management Agency. HAZUS-MH MR4 technical manual. Natl Inst Build Sci Fed Emerg Manag Agency (NIBS FEMA). 2003:712.
51. Choi H, Erochko J, Christopoulos C, Tremblay R. Comparison of the seismic response of steel buildings incorporating self-centering energy-dissipative braces, buckling restrained braces and moment-resisting frames. *Research Report 05-2008*.
52. Andrews BM, Song J, Fahnestock LA. Assessment of buckling-restrained braced frame reliability using an experimental limit-state model and stochastic dynamic analysis. *Earthq Eng Eng Vib*. 2009;8:373-385. doi:10.1007/s11803-009-9013-8
53. McCormick J, Aburano H, Ikenaga M, Nakashima M. Permissible residual deformation levels for building structures considering both safety and human elements. in: 14th World Conf. Earthq. Eng., Beijing, China, 2008:8.
54. Iwata Y, Sugimoto H, Kuwamura H. Reparability limit of steel structural builidings : study on performance based design of steel structural buildings, Part 2. *J Struct Constr Eng*. 2005;70:165-172. doi:10.3130/aijs.70.165_1

How to cite this article: Gutiérrez-Urzúa F, Freddi F. Influence of the design objectives on the seismic performance of steel moment resisting frames retrofitted with buckling restrained braces. *Earthquake Engng Struct Dyn*. 2022;51:3131–3153. https://doi.org/10.1002/eqe.3717